

**SOLID STATE NMR STRUCTURAL CHARACTERIZATION OF
SELF-ASSEMBLING PEPTIDE ANALOGUES**

A Dissertation
Presented to
The Academic Faculty

by

Benjamin Hudson

In Partial Fulfillment
of the Requirements for the Degree
Chemical Engineering Doctorate of Philosophy in the
School of Chemical and Biomolecular Engineering

Georgia Institute of Technology
DECEMBER 2018

COPYRIGHT © 2018 BY BENJAMIN HUDSON

SOLID STATE NMR STRUCTURAL CHARACTERIZATION OF SELF-ASSEMBLING PEPTIDE ANALOGUES

Approved by:

Dr. Anant Paravastu, Advisor
School of Chemical and Biomolecular
Engineering
Georgia Institute of Technology

Dr. Martha Grover
School of Chemical and Biomolecular
Engineering
Georgia Institute of Technology

Dr. Andreas Bommarius
School of Chemical and Biomolecular
Engineering
Georgia Institute of Technology

Dr. Raquel Lieberman
School of Chemistry and Biochemistry
Georgia Institute of Technology

Dr. Julie Champion
School of School of Chemical and
Biomolecular Engineering
Georgia Institute of Technology

Date Approved: [October 23, 2018]

This is dedicated to my Lord, Jesus Christ, in whom I know true freedom.

ACKNOWLEDGEMENTS

I would like to first acknowledge my thesis advisor, Dr. Anant Paravastu, who never once wavered in the belief that I would finish this journey and always supported my scientific endeavors (even when he didn't think they would work). Thank you for inviting me to come with you to Atlanta. And finally, thank you for all the coffee! Thank you also to the rest of the research group. I'm glad to have been able to work with each and every one of you. I'll miss you all come Monday morning group meetings next semester.

I'd also like to thank my community at Blueprint Church. You all have been a huge help to me in staying grounded through this whole process. I can't imagine where I'd be right now if Chris hadn't struck up a conversation with me about three years ago (because Adrienne told him to), but I'm not sure if I would have ever been able to write these acknowledgments if you hadn't.

Finally, I'd like to say thank you to my Mom and Dad back in Florida. I know you may not have been excited about me moving away to go to school in Atlanta, but you were always supportive of my decision and understood my reasons for wanting to go. I couldn't have done it without both of you.

TABLE OF CONTENTS

ACKNOWLEDGEMENTS	iv
LIST OF FIGURES	vii
LIST OF SYMBOLS AND ABBREVIATIONS	xi
SUMMARY	xii
CHAPTER 1. Introduction	1
1.1 Peptide Structure	1
1.1.1 Peptide Primary Structure	1
1.1.2 Peptide Secondary Structure	2
1.2 Peptide Self-Assembly	3
1.2.1 Designer Peptide Self-Assembly	4
1.3 Self-Assembling Peptide Analogues	4
1.3.1 Peptide Analogues	4
1.3.2 Peptoids	5
1.3.3 Low Molecular Weight Gelators	6
CHAPTER 2. Materials and methods	8
2.1 Solid-State Nuclear Magnetic Resonance	8
2.1.1 One-Dimensional Cross Polarization Magic Angle Spinning NMR	9
2.1.2 PITHIRDS-CT Dipolar Recoupling NMR	10
2.1.3 Finite Pulse Radio Frequency Dipolar Recoupling NMR	10
2.1.4 Two-Dimensional Carbon-Hydrogen-Hydrogen-Carbon NMR	11
2.2 NMR Spin Simulations	11
2.3 Fourier-Transform Infrared Spectroscopy	12
2.4 Peptoid B28 Sample Preparation	12
2.5 Fmoc-FF Sample Preparation	12
2.5.1 Hydrogel Preparation	13
2.5.2 NMR Sample Preparation	13
2.6 Molecular Modeling	14
2.6.1 Peptoid B28	14
2.6.2 Fmoc-FF	14
CHAPTER 3. Research Aim: Peptoid B28	16
3.1 Background and Introduction	16
3.1.1 Peptoid B28	16
3.1.2 Previous Peptoid B28 Structural Measurements	18
3.1.3 Introduction to Research Aims	19
3.2 Results and Discussion	20
3.2.1 Solid-State NMR	20
3.2.2 Molecular Modelling	25

CHAPTER 4. Research Aim: fmoc-ff	30
4.1 Background and Introduction	30
4.1.1 Fmoc-FF	30
4.1.2 Previous Fmoc-FF Structural Measurements	32
4.1.3 Introduction to Research Aims	34
4.2 Results and Discussion	35
4.2.1 Solid-State NMR	35
4.2.2 Molecular Modeling	44
4.2.3 FTIR	46
CHAPTER 5. Conclusions and future work	49
5.1 Peptoid B28	49
5.2 Fmoc-FF	51
5.3 Final Summary	54
CHAPTER 6. Appendix	56
6.1 NMR Pulse Sequences	56
6.1.1 CPMAS	56
6.1.2 CHHC	57
6.1.3 fpRFDR	57
6.1.4 CHHC	58
6.2 Peptoid B28 Supplemental Figures	58
6.3 Fmoc-FF Supplemental Figures	60
REFERENCES	64

LIST OF FIGURES

Figure 1	– Standard amino acid primary structure and formation of a peptide bond. Four examples of amino acid ‘R’ groups are provided.	12
Figure 2	– Cartoon examples of peptide secondary structure. A right-handed α -helix is shown in blue and an antiparallel β -sheet in green.	13
Figure 3	– Backbone torsion angles ϕ , ψ , and ω are shown in blue, red, and green, respectively. Angles of rotation are positive with respect to the α -carbon in ϕ and ψ and positive with respect to the carbonyl in ω .	13
Figure 4	– Schematic showing the distinction between peptoid and peptide primary structure.	16
Figure 5	– Primary structure of peptoid B28 with the aminoethyl block in blue brackets and the carboxyethyl block in red brackets.	27
Figure 6	– TEM image of peptoid B28 nanosheets.	28
Figure 7	– Planar representations of peptoid backbone amide bonds in the <i>cis</i> (A) and <i>trans</i> (B) configurations.	30
Figure 8	– CPMAS spectra of peptoid B28 nanosheets showing ^{13}C natural abundance signals corresponding to a well-ordered structure.	31
Figure 9	– Comparison of <i>cis</i> and <i>trans</i> configurations and their respective $\text{C}\alpha$ - $\text{C}\alpha$ distance distribution estimates from molecular dynamics simulations of peptoid B28 monomer units (single molecules).	32
Figure 10	– A) Unabbreviated primary structure of peptoid B28 with ^{13}C -labeled $\text{C}\alpha$ pairs identified by black triangles (6, 7), red triangles (7, 8), and green triangles (14, 15). B) PITHIRDS-CT data for $\text{C}\alpha$ pairs (6, 7) and (7, 8). Nanosheet (<i>cis</i>) decays are indicated by filled triangles, and amorphous control (<i>trans</i>) decays are indicated by empty triangles. C) PITHIRDS-CT decays from nanosheet (filled triangles) and amorphous control samples (empty triangles) labeled at (14, 15). Color scheme for (B) and (C) is maintained from (A). Simulated curves are shown to indicate predicted PITHIRDS-CT decays for distance distributions corresponding to 100% <i>cis</i> , 80% <i>cis</i> , 20% <i>cis</i> , and 0% <i>cis</i> in (B) and 40% <i>cis</i> , and 0% <i>cis</i> in (C).	33

Figure 11	– A) <i>Cis</i> Σ -strand configuration. B) <i>Trans</i> Σ -strand configuration. Length/residue and total molecular length values were obtained through molecular dynamics simulation of peptoid nanosheets.	35
Figure 12	– Illustration showing the preference for <i>trans</i> in the unassembled state and <i>cis</i> in the nanosheet state.	37
Figure 13	– A) Side-view and B) top view of new <i>cis</i> nanosheet model. N-(2-aminoethyl) residues are shown in red, N-(2-carboxyethyl) residues in black, and N-(2-phenylethyl) residues in black.	38
Figure 14	– Evolution of $ \omega $ of each residue over all B28 chains in a biased simulation was an all- <i>cis</i> nanosheet. The middle residue shows a near equal distribution of <i>cis</i> and <i>trans</i> .	38
Figure 15	– Primary Structure of Fmoc-FF.	41
Figure 16	– (A-F) Confocal microscopy images of Fmoc-FF gels in: A) DMSO/H ₂ O, B) acetone/H ₂ O, C) methanol/H ₂ O, D) HFIP/H ₂ O, E) benzene, and F) toluene. Scale bars represent 10 μ m. (G-I) TEM images of Fmoc-FF gels in G) DMSO/H ₂ O, H) methanol/H ₂ O, and I) toluene.	44
Figure 17	– A) CPMAS spectra obtained from Fmoc-FF nanofibers self-assembled in 5% DMSO (black), 5% methanol (blue), 80% methanol (green), and toluene (red). B) carbonyl, C) γ -carbon, and D) α -carbon signals from each spectrum.	47
Figure 18	– Side-by-side comparison of CHHC (A) and fpRFDR (B) spectra for Fmoc-FF nanofibers assembled in 5% DMSO. Red circles highlight α -carbon signals, orange circles show β -carbon signals, blue circles show α - α correlation signals, and green circles show α - β correlation signals. Correlation signals are mirrored on each side of the diagonal containing α -carbon and β -carbon signals.	51
Figure 19	– Side-by-side comparison of CHHC (A) and fpRFDR (B) spectra for Fmoc-FF nanofibers assembled in 10% methanol. Red circles highlight α -carbon signals, orange circles show β -carbon signals, blue circles show α - α correlation signals, and green circles show α - β correlation signals. Correlation signals are mirrored on each side of the diagonal containing α -carbon and β -carbon signals.	51
Figure 20	– Side-by-side comparison of CHHC (A) and fpRFDR (B) spectra for Fmoc-FF nanofibers assembled in 80% methanol. Red circles highlight α -carbon signals, orange circles show β -carbon signals, blue circles show α - α correlation signals, and green circles show α -	52

	β correlation signals. Correlation signals are mirrored on each side of the diagonal containing α -carbon and β -carbon signals.	
Figure 21	– Side-by-side comparison of CHHC (A) and fpRFDR (B) spectra for Fmoc-FF nanofibers assembled in toluene. Red circles highlight α -carbon signals, orange circles show β -carbon signals, blue circles show α - α correlation signals, and green circles show α - β correlation signals. Correlation signals are mirrored on each side of the diagonal containing α -carbon and β -carbon signals.	52
Figure 22	– Overlay of one-dimensional slices from CHHC and fpRFDR spectra from A) 5% DMSO, B) 10% methanol, C) 80% methanol, and D) toluene.	53
Figure 23	– A) Overlay of CHHC spectra from Fmoc-FF formed in 10% methanol using 100% ^{13}C -labeled material (black) and 50/50 ^{13}C labeled/unlabeled (red). B) One-dimensional slice comparison at 58 ppm from both spectra in (A).	54
Figure 24	– A) Idealized, parallel diphenylalanine backbone, B) Idealized, antiparallel diphenylalanine backbone, C) Idealized, flipped antiparallel diphenylalanine backbone, and D) Smith diphenylalanine backbone. Dashed lines indicate hydrogen bonds, solid black lines indicate intermolecular $\text{H}\alpha$ pairs outside CHHC detection range, red lines indicate intramolecular $\text{H}\alpha$ pairs, and green lines indicate intermolecular $\text{H}\alpha$ pairs inside CHHC detection range. All distances are given in angstroms (\AA).	55
Figure 25	– FTIR spectra from Fmoc-FF formed in 5% DMSO (black), 10% methanol (blue), 80% methanol (green), and toluene (red).	57
Figure A1	– CPMAS pulse sequence	66
Figure A2	– PITHIRDS-CT pulse sequence	67
Figure A3	– fpRFDR pulse sequence	67
Figure A4	– CHHC pulse sequence	68
Figure A5	– CPMAS spectra of peptoid B28 nanosheets with 100% ^{13}C isotopic labeling at the sites indicated.	68
Figure A6	– Comparison of PITHIRDS-CT data to simulated curves that consider potential effects of intermolecular ^{13}C - ^{13}C dipolar couplings. Symbols correspond to measured PITHIRDS-CT decays for peptoid B28 nanosheets labeled at the sixth and seventh α -carbon sites specified in Figure 4. The curve for the 2-spin simulation corresponds to adjacent ^{13}C -atoms on either side of an	69

amide bond in the *cis* configuration, with the distribution of internuclear distances shown in Figure 3. The 10-spin simulations were performed to evaluate the maximum possible effects of inter-molecular ^{13}C - ^{13}C dipolar couplings, and correspond to pairs of ^{13}C atoms separated by an intramolecular distance, d , of either 3\AA (*cis* configuration) or 3.8\AA (*trans* configuration). The 10-spin simulations each include 5 pairs of ^{13}C atoms, with each pair separated by an intermolecular distance of 4.5\AA . The 4.5\AA estimate corresponds to distance between adjacent molecular backbones within the same molecular monolayer observed with aberration-corrected TEM images and x-ray diffraction measurements on similar nanosheet forming peptoids. This distance corresponds to a lower limit for intermolecular ^{13}C - ^{13}C distances and therefore maximal possible intermolecular ^{13}C - ^{13}C dipolar couplings. In our view, a 4.5\AA distance between ^{13}C -labeled sites on adjacent molecules corresponds to inter-molecular alignments that are unlikely to occur because like-charged segments of peptoid B28 are unlikely to align in this way. Comparison of the 2-spin and 10-spin simulated PITHIRDS-CT decays indicates that inter-molecular ^{13}C - ^{13}C dipolar couplings did not affect the results for ^{13}C - ^{13}C dipolar recoupling times under 10 ms. Our assessments of amide bond isomerization are thus based on the shapes of curves corresponding to dipolar recoupling times below 10 ms.

- | | | |
|------------|---|----|
| Figure A7 | – CPMAS of unlabeled Fmoc-FF (black) and Fmoc-FF with uniform ^{13}C , ^{15}N (red). Both Fmoc-FF samples were assembled in 5% DMSO. Peaks appearing in the black spectrum but not the red spectrum originate from the Fmoc group. They are assigned using chemical shift standards from molecules with similar local chemical bonding. | 70 |
| Figure A8 | – Reprinted FTIR spectra from Zhou (top left), Ryan (top right), Jayawarna (bottom left), and Smith (bottom right). The green line in each spectrum marks the position of the amide I stretch. These spectra were used to conclude that Fmoc-FF forms an anti-parallel β -sheet. | 71 |
| Figure A9 | – Reprinted FTIR spectra from Mu. These spectra were used to conclude that Fmoc-FF assemblies are disordered in the FF subunit of the molecule. | 72 |
| Figure A10 | – fpRFDR spectra from Fmoc-FF formed in 10% methanol. The off-diagonal correlation signals indicate that our CHHC contacts are between F1 and F2 of the FF subunit. | 73 |

LIST OF SYMBOLS AND ABBREVIATIONS

CD	Circular Dichroism
Fmoc-FF	Fluorenylmethoxycarbonyl-Diphenylalanine
MAS	Magic Angle Spinning
NMR	Nuclear Magnetic Resonance
TEM	Transmission Electron Microscopy
CPMAS	Cross Polarization Magic Angle Spinning
fpRFDR	Finite Pulse Radio Frequency Dipolar Recoupling
CHHC	Carbon Hydrogen Hydrogen Carbon
NAMD	Nanoscale Molecular Dynamics
A β	Amyloid- β , the Alzheimer's peptide

SUMMARY

Portions of this work have been adapted with permission from:

Hudson, B. C.; Battigelli, A.; Connolly, M. D.; Edison, J.; Spencer, R. K.; Whitlam, S.; Zuckermann, R. N.; Paravastu, A. K. Evidence for Cis Amide Bonds in Peptoid Nanosheets. *J. Phys. Chem. Lett.* 2018, 9, 2574-2578.

Edison, J. R.; Spencer, R. K. Butterfoss, G. L.; **Hudson, B. C.**; Hochbaum, A. I.; Paravastu, A. K.; Zuckermann, R. N.; Whitlam, S. Conformations of Peptoids in Nanosheets Result from the Interplay of Backbone Energetics and Intermolecular Interactions. *P. Natl. Acad. Sci. USA.* 2018, 115, 5647-5651.

Dudukovic, N.; **Hudson, B. C.**; Paravastu, A. K.; and Zukoski, C. “Self-assembly Pathways and Polymorphism in Peptide-Based Nanostructures.” *Nanoscale* 10, 1508-1516 (2018).

Huang D., **Hudson B. C.**, Gao Y., Roberts E. K., and Paravastu A. K. (2018) Solid-State NMR Structural Characterization of Self-Assembled Peptides with Selective ¹³C and ¹⁵N Isotopic Labels. Nilsson B., Doran T. (eds) *Peptide Self-Assembly. Methods in Molecular Biology*, vol 1777. Humana Press, New York, NY.

Research in the field of designer nanostructure has shown great potential for use of peptides, peptide analogues, and a wide array of small molecules in a variety of industries and applications. As the field continues to expand, the need for techniques which are capable of providing structural detail at atomic-level resolution will only grow. The question of how best to extract atomic-level structural detail from these systems has yet to be adequately addressed, however. Here I show the efficacy of solid-state nuclear magnetic resonance (NMR) in extracting molecular-level detail from two self-assembling peptide analogues: peptoid B28 and fluorenylmethoxycarbonyl-diphenylalanine (Fmoc-FF). A study of peptoid B28 nanosheets has shown the capability of dipolar recoupling solid-state NMR to distinguish between the *cis* and *trans* configurations of peptoid backbone amide bonds, providing refined physical constraints for an evolving B28 nanosheet molecular model and revealing previously unconsidered peptoid backbone folding behavior. My

study of Fmoc-FF suggests this system is highly polymorphic despite its small size, and that the polymorphism appears to be dependent on solvent environment. Despite this polymorphism however, two-dimensional solid-state NMR indicates each of our Fmoc-FF systems feature a common backbone hydrogen-bonding pattern of diphenylalanine sidechains inconsistent with the most widely accepted Fmoc-FF nanofiber model.

Solid-state NMR has never been applied either peptoid B28 or Fmoc-FF, nor is there any evidence in the literature that it has ever been applied a peptoid system or Fmoc-dipeptide. I am borrowing these solid-state NMR experiments from peptide characterization methods and applying them to probe for structural phenomena that has never been tested in either system. I have simply looked at the proposed molecular arrangements in both peptoid B28 and Fmoc-FF and applied measurements sensitive to the details I want to see. This is a not a standard application of solid-state NMR, but nothing new ever began as standard.

CHAPTER 1. INTRODUCTION

The aim of the work presented herein has been to demonstrate the novel application of established solid-state NMR techniques to address long-standing knowledge gaps and unexpected behavior in self-assembling peptide analogue systems. This section will provide background information dealing with peptide structure, peptide self-assembly, peptide analogues, and classes of self-assembling peptide analogues on which this work is focused. Target self-assembling systems will be addressed in their respective research aim chapters.

1.1 Peptide Structure

1.1.1 Peptide Primary Structure

Peptides are compounds made up of two or more amino acids, with each amino acid possessing the same basic structure. There are twenty naturally occurring amino acids, from which all naturally occurring proteins are composed. Each is listed here, along with their primary structures and accepted abbreviations.¹ All amino acids have the same basic structure: a central α -carbon atom is bound to a carboxylic acid, amine, hydrogen, and a unique 'R' group. Amino acids are distinguished from one another by their 'R' groups, with the folding and functionality of the peptides being determined by the amino acid sequence. Two amino acids bond via a dehydration reaction between their amine and carboxylic acid groups. Peptides are distinguished from proteins by size, with peptide sequences being <50 amino acids in length. Figure 1 shows a summary of amino acid and peptide primary structure.

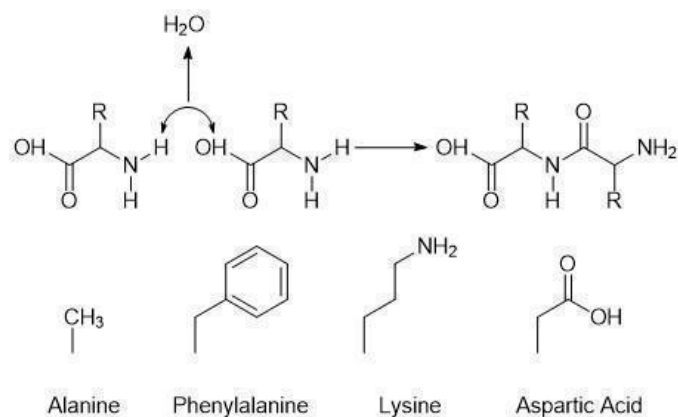


Figure 1 – Standard amino acid primary structure and formation of a peptide bond. Four examples of amino acid ‘R’ groups are provided.

1.1.2 Peptide Secondary Structure

Peptide secondary structure refers to the physical orientation adopted by a single peptide strand. The two basic peptide secondary structures are the α -helix and β -sheet, shown in Figure 2, which can be either left or right-handed and parallel or antiparallel, respectively. These structures are stabilized by hydrogen bonding between amide nitrogen and carbonyl groups along the peptide backbone (intra-strand bonding in α -helices and inter-strand bonding in β -sheets). Peptide secondary structure is also characterized in terms of the torsion angles identified in Figure 3: ϕ , ψ , and ω . For α -helices, typical ϕ and ψ values are about -60° and -40° for right-handed helices and 45° for both ϕ and ψ in left-handed helices. For β -sheets, typical ϕ and ψ values are about -120° and 105° in a parallel conformation and -145° and 140° in an antiparallel configuration. In all standard peptide configurations, the backbone amide bond is in the *trans* configuration, corresponding to an ω value of 180° . The *trans* configuration of the backbone amide bond in peptides is heavily energetically favoured over the *cis* configuration.²

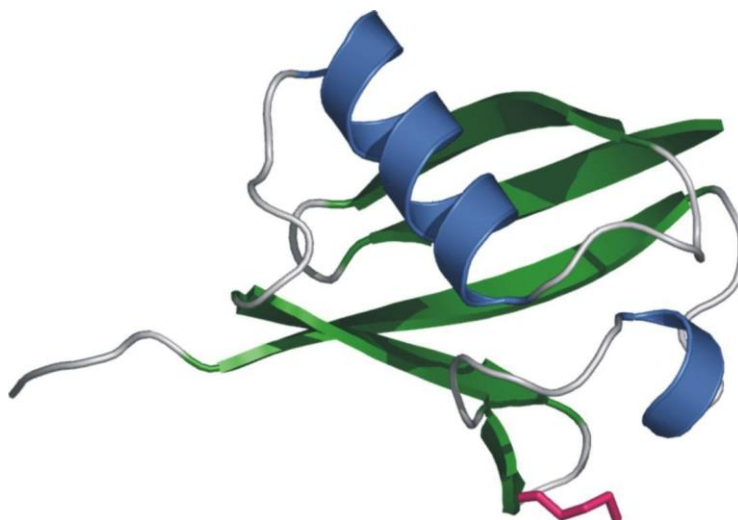


Figure 2 – Cartoon examples of peptide secondary structure. A right-handed α -helix is shown in blue and an antiparallel β -sheet in green.

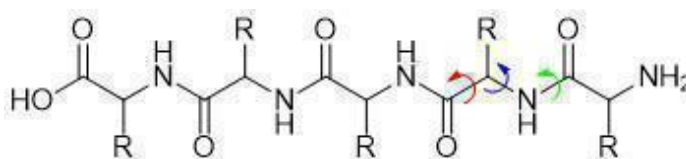


Figure 3 – Backbone torsion angles φ , ψ , and ω are shown in blue, red, and green, respectively. Angles of rotation are positive with respect to the α -carbon in φ and ψ and positive with respect to the carbonyl in ω .

1.2 Peptide Self-Assembly

Peptide self-assembly is the spontaneous organization of identical peptide monomers into highly ordered assemblies. The assemblies are bound together through non-covalent interactions such as electrostatic forces, hydrogen bonding, and π - π stacking. Peptide self-assembly is a hallmark of many neurodegenerative diseases (e.g. Alzheimer's, Parkinson's, and amyotrophic lateral sclerosis), in which self-assembled peptide structures aggregate into plaques on the surface of nervous tissues.³ In particular, the Paravastu group has done considerable work in identifying structures formed by the Alzheimer's peptide, amyloid- β .⁴⁻⁵

1.2.1 Designer Peptide Self-Assembly

Alongside naturally occurring self-assembling peptides we have self-assembling designer peptides. Designer peptide self-assembly refers to *de novo* design of a peptide monomer unit which will self-assemble into well-ordered structure upon introduction to specific environmental conditions (often a buffer with a specific salt concentration). The original designer peptides were developed in the early 1990's and were based a self-assembling segment of the yeast protein, Zuotin.⁶⁻⁷ This segment, EAK16, is sixteen amino acids in length and composed of alternating hydrophilic and hydrophobic amino acids (AEAEAKAKAEAEAKAK). The hydrophilic amino acids glutamic acid (E) and Lysine (K) alternate in a (--++) pattern. CD spectra from EAK16 in water is characteristic of a β -sheet, and self-assembly occurs upon introduction of salt to the solution.

From the study of EAK16 came the first true designer self-assembling peptide system, RAD16 (RARARADARARADADA).⁸ The design featured alternating hydrophobic and hydrophilic amino acids, a charge motif similar to EAK16 (--++ for EAK16 and +++- for RAD16), exchanged glutamic acid (E) for aspartic acid (D) and lysine (K) for arginine (R), and was found to self-assemble under similar conditions to EAK16. This approach, which features patterns of hydrophilicity and hydrophobicity in the amino acid R-groups and positive and negative charge patterning in the hydrophilic groups, has become a cornerstone in designer, β -sheet forming, self-assembling peptides.

1.3 Self-Assembling Peptide Analogues

1.3.1 Peptide Analogues

The field of designer self-assembly has been propelled forward by growth of the peptide industry because it has made any imaginable peptide sequence commercially available. Because of this commercial availability and our current collective knowledge of synthetic chemistry, there was no reason from a non-biological perspective for the “building materials” of designer nanostructure to be limited to amino acids. Along this vein, many research groups have begun to design non-naturally occurring self-assembling molecular systems such as peptoids and low molecular weight gelator molecules. These systems are heavily influenced by known peptide folding and assembly properties, but are also distinct from peptide primary structure⁹⁻¹⁰. Thus far these peptide analogue systems have not been highly relevant to study of pathology. However, they are highly relevant to design of nanostructure.

1.3.2 Peptoids

Peptoids are peptide-mimetic, sequence-defined heteropolymers that can form highly ordered crystals in the solid state and protein-like supramolecular assemblies in aqueous solution¹¹⁻¹³. Their folding and assembly are influenced by the sequence of chemically diverse sidechains along an *N*-substituted glycine backbone. Peptoid residues are polymerized iteratively with precise sequence control via solid-phase synthesis techniques that are analogous to peptide synthesis techniques¹⁴. A comparison of peptoid and primary structure is shown in Figure 4.

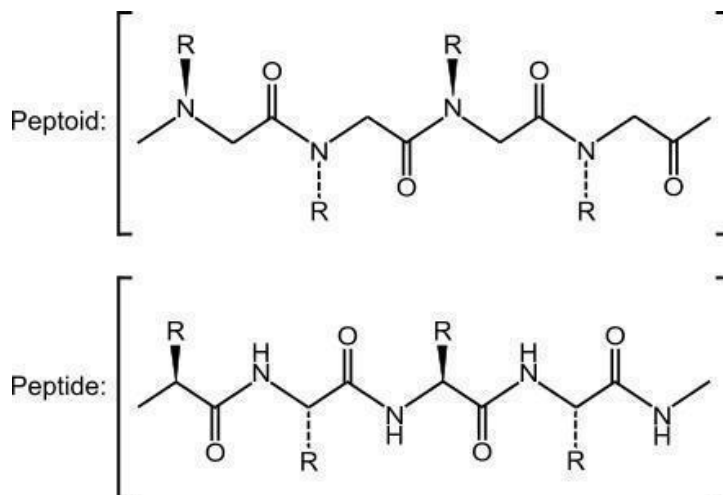


Figure 4 – Schematic showing the distinction between peptoid and peptide primary structure.

The potential for peptoid mimicry of proteins has already been demonstrated in studies of lung surfactant proteins SP-B and SP-C.¹²⁻¹³ Without these proteins, respiratory distress syndrome occurs. Using submonomer units with properties and structures similar to those of the corresponding amino acid side chains on the surfactant proteins, researchers were able to produce peptoids which mimicked the folding and function of the native proteins. These peptoids have been used to successfully treat respiratory distress syndrome in infants.

1.3.3 Low Molecular Weight Gelators

Low molecular weight gelator (LMWG) molecules have emerged as a growing topic of research in recent years. LMWG's are small molecules, typically with molecular weight < 1000 Da, which self-assemble into macromolecular anisotropic structures (often nanofibers).¹⁵ At sufficiently high concentration, the nanofiber assemblies create an entangled network capable of supporting a gel state. These gels have been the primary

focus in a number of studies exploring topics including three-dimensional cell culture¹⁶⁻¹⁸, directed stem cell differentiation¹⁹⁻²⁰, development of electrically conductive gels²¹⁻²², and targeted drug delivery.²³⁻²⁵

One of the pioneers of low molecular weight gelator technology, Rein Ulijn, founded the company Biogelx. Biogelx specializes in many of the applications for synthetic peptide hydrogels mentioned in the previous paragraph. They also authored a book chapter in Peptide Self-Assembly regarding three-dimensional cell culture on self-assembling peptide hydrogels.²⁶ This is the same book in which the Paravastu group published a book chapter on solid-state NMR of self-assembling peptides.²⁷

CHAPTER 2. MATERIALS AND METHODS

This chapter will deal specifically with my primary and supplementary analytical methods, as well as specific material preparation methods for my research aims.

2.1 Solid-State Nuclear Magnetic Resonance

My main experimental technique is solid-state nuclear magnetic resonance (NMR). NMR measures the strength and variations of the local magnetic field experienced by magnetically susceptible nuclei. These magnetic fields contain valuable information about the local electronic environment of individual nuclear spins. The nuclear spins of interest in my work will be ^1H (99.9% natural abundance) and ^{13}C (1.1% natural abundance). To enhance signal from isotopes with low natural abundance, NMR samples may be synthesized with specific “isotopic labeling” schemes, in which abundant and NMR-inactive ^{12}C atoms at desired sites are replaced with their respective magnetically susceptible isotope, ^{13}C . For examples of NMR spectra, please refer to my research aims and the Paravastu group’s published book chapter, which covers all of our commonly used solid-state NMR techniques and their standard spectrometer setups.²⁷

Solid-state NMR is a useful means of probing molecular conformation in materials such as peptoid B28 and Fmoc-FF which form assemblies too large to tumble isotropically in solution but also do not precipitate. The impaired diffusivity of such systems leads to anisotropies in the local magnetic environment of otherwise equivalent nuclei, making solution-state NMR impractical. Lyophilization is used to remove solvent from the system, leaving only the supramolecular assembly behind. Once the sample is dry, solid-state NMR

may be used to probe molecular conformation of the assemblies present. Local anisotropies are averaged away using solid state NMR specific techniques, magic angle spinning (MAS) and spin decoupling. The averaging techniques allow us to greatly increase the resolution of NMR spectra obtained from solid samples, though standard systems do not approach the resolution seen in solution-state NMR.

2.1.1 One-Dimensional Cross Polarization Magic Angle Spinning NMR

Each of my studies will begin with ^1H - ^{13}C cross polarization magic angle spinning (CPMAS) NMR.²⁸ This is a double resonance experiment, meaning it excites two different nuclear species, ^1H and ^{13}C in this case. The result of the experiment is a spectrum representative of all ^{13}C frequencies in a sample. The frequencies are shown in a 0-200 parts-per-million (ppm) range with general rules for peak assignments as follows: carbonyl carbons appear in the 160-180 ppm range, aromatic carbons in the 100-150 ppm range, and aliphatic carbons in the 20-70 ppm range. The ppm scale refers to deviation (in Hz) from a standard ^{13}C frequency, usually tetramethylsilane (measured in MHz). Because the natural abundance of ^{13}C is approximately 1.1%, the spectrum we collect from unlabeled material is the collective signal of approximately 1.1% of all carbon atoms in the sample. While this large sample size does not give us precise details of structural arrangement, we are able to make assumptions regarding the degree of molecular order. Sharp, distinct signals well above the spectral noise indicate large populations of carbon atoms experiencing very similar local electronic environments. This is what we see in systems exhibiting a high degree of molecular order and is a requirement for further study using NMR. Once the presence of a well-ordered assembly has been established, we proceed with synthesis of isotopically labeled NMR samples for more the specialized solid-state NMR experiments

described below. All CPMAS spectra shown in this document were obtained using an 11.75 T spectrometer with either 20 or 25 kHz MAS. The CPMAS NMR pulse sequence is shown in Figure A1 of the appendix. All further solid-state NMR measurements discussed in herein require enrichment with ^{13}C isotopes at the sites of interest. Isotopic labeling patterns for specific materials and samples will be detailed in the research aims chapter.

2.1.2 *PITHIRDS-CT Dipolar Recoupling NMR*

I will make interatomic distance approximations using the NMR experiment, PITHIRDS-CT.²⁹ PITHIRDS-CT is a homonuclear dipolar recoupling experiment which may be used with either ^{13}C or ^{15}N spin pairs. Under magic angle spinning conditions, dipolar couplings are averaged away, meaning these signals do not appear in the spectra. Dipolar recoupling experiments are able to selectively reintroduce these couplings and yield a time-dependent NMR signal. The strength of the dipolar coupling between the spin pair scales with $1/r^3$, where r is inter-nuclear distance. The experimental NMR parameters are the same as those employed in previous studies by the Paravastu group (12.5 kHz magic angle spinning, 11.75 T spectrometer), with the exception of the total recoupling time, which was 30.72 ms. In the terms defined by Tycko, $k_2 + k_3 = 16$. The PITHIRDS-CT pulse sequence is shown in Figure A2 of the appendix.

2.1.3 *Finite Pulse Radio Frequency Dipolar Recoupling NMR*

Finite pulse radio frequency dipolar recoupling (fpRFDR) is a two-dimensional solid-state NMR experiment which probes for direct dipolar couplings between ^{13}C nuclei. The experiment is designed to detect couplings out to an approximate distance of 1.5 Å and is commonly used to map out correlations between directly bonded carbon atoms. I

will be using fpRFDR as a control experiment with carbon-hydrogen-hydrogen-carbon (CHHC) NMR, which is described subsequently. The fpRFDR pulse sequence is shown in Figure A3 in the appendix.

2.1.4 *Two-Dimensional Carbon-Hydrogen-Hydrogen-Carbon NMR*

Carbon-hydrogen-hydrogen-carbon (CHHC), like fpRFDR, is another two-dimensional solid-state NMR experiment. CHHC however, is designed to detect ^{13}C - ^{13}C correlations between the carbon atoms of two specifically aligned CH-groups in which the ^1H nuclei are positioned within approximately 3 Å of one another.³⁰ The experiment induces magnetization transfer beginning from one of the ^{13}C nuclei to the directly bonded ^1H nucleus. Spin diffusion then occurs between ^1H nuclei of the CH groups, then cross polarization between the ^1H and ^{13}C nuclei of the second CH group. In the case of anti-parallel β -sheet forming peptides, this unique alignment appears between the α -carbon atoms of adjacent peptide backbones within the β -sheet. The same contact does not appear in parallel β -sheets, allowing spectroscopists to use CHHC as a means of differentiating between the two secondary structures. CHHC contacts may also be observed between CH groups in which the carbon atoms are directly bonded. To differentiate between CHHC contacts of directly bonded atoms and anti-parallel β -sheet contacts, we use fpRFDR, which will reveal interaction between directly bonded carbon atoms but not the anti-parallel β -sheet contacts. The CHHC pulse sequence is shown in Figure A4 in the appendix.

2.2 **NMR Spin Simulations**

I used SpinEvolution® NMR simulation software to generate predicted PITHIRDS-CT curves for interatomic distances ranging 0.275nm to 0.410nm. The

simulated curves will be used in approximating the interatomic distance associated with experimental PITHIRDS-CT curves.³¹

2.3 Fourier-Transform Infrared Spectroscopy

Fourier-transform infrared spectroscopy (FTIR) measurements were performed using a Shimadzu Prestige 21 spectrometer. Each spectrum was obtained from 45 scans/measurement at a resolution of 16.0 cm⁻¹. Fmoc-FF hydrogel samples were placed directly on to the IR probe and held in place using a sample press which was part of the Shimadzu instrumentation.

2.4 Peptoid B28 Sample Preparation

All peptoid B28 samples were produced by synthetic chemists using a well-established solid-phase, sub-monomer synthesis method at the Molecular Foundry user facility at the Lawrence Berkeley National Laboratory in Berkeley, CA.^{14, 32} Nanosheet samples were assembled using a scaled up vial rocking method¹⁴, and the amorphous control samples were obtained from lyophilization of the B28 peptoid from acetonitrile/water (1:1, v/v). It was my responsibility to communicate with the team in Berkeley and determine the most effective placement of isotopic labels from their accessible sites.

2.5 Fmoc-FF Sample Preparation

All Fmoc-FF used in this research was purchased from Bachem at >99% purity. My study focused on Fmoc-FF nanofiber hydrogels formed in 5% DMSO, 5% methanol,

10% methanol, 80% methanol, and toluene. All solvent percentages are given as $\frac{\text{solvent volume}}{\text{total volume}}$ in water.

2.5.1 Hydrogel Preparation

Fmoc-FF hydrogels in 5% DMSO, 5% methanol, 10% methanol, and 80% methanol were prepared using a solvent switch method. First, Fmoc-FF was dissolved in the pure solvent. Fmoc-FF fully dissolved in DMSO at room temperature. Dissolution of Fmoc-FF in methanol required heating the system to approximately to 40°C. After complete dissolution, each sample was diluted with water to a final Fmoc-FF concentration of 15 mg/mL and the desired solvent volume fraction (5% DMSO, 10% methanol, or 80% methanol). Upon dilution with water, each system immediately began to transition from the solution state to the gel state. Samples formed in 5% DMSO, 5% methanol, and 10% methanol were left to equilibrate over a 24-48 hour period. Samples in 80% methanol were only allowed to equilibrate for approximately 8 hours. If left to equilibrate overnight, Fmoc-FF in 80% methanol would crystallize. Fmoc-FF hydrogels in toluene were formed by mixing Fmoc-FF in toluene at a concentration of 15 mg/mL and heating the sample to approximately 80°C to induce dissolution of the Fmoc-FF. Upon complete dissolution, the sample was removed from the heat source. Gelation began immediately upon cooling. Toluene hydrogels were left to equilibrate for 24-48 hours.

2.5.2 NMR Sample Preparation

I produced solid-state NMR samples from the DMSO and methanol gels by first freezing the gels in liquid nitrogen then lyophilizing the solvents from the frozen gels. In

the case of 80% methanol gels, I carried out a solvent exchange by depositing 1 mL H₂O on top of the gel to allow for exchange with the methanol. The water was refreshed every 15 minutes over the course of 2.5 hours. After the solvent exchange, the sample was lyophilized. NMR samples from toluene gels were produced by allowing the toluene to evaporate from the gel under a hood at room temperature.

Because of the discrepancies in NMR sample drying methods, I prepared NMR control samples from 80% methanol and toluene by freezing gels in liquid nitrogen and drying them using a lyophilizer with a temperature-controlled drying chamber. Each of the drying procedures described for 80% methanol and toluene produced NMR samples with consistent NMR spectra obtained from lyophilized samples, suggesting no structural variation due to drying method. We also have no evidence to suggest lyophilization compromises the self-assembled fiber structure.

2.6 Molecular Modeling

2.6.1 *Peptoid B28*

Molecular modelling of peptoid B28 nanosheets was performed using Nanoscale Molecular Dynamics (NAMD)³³ package together with the MFTOID forcefield developed at the Molecular Foundry.³⁴

2.6.2 *Fmoc-FF*

All novel Fmoc-FF structures are idealized images drawn using Visual Molecular Dynamics (VMD) and the molefactory plugin and manipulated using Mathematica™. Each structure has a 4.8 Å intermolecular distance, which is standard for β-strands within a β-

sheet. Each molecule also has the standard (ϕ, ψ) β -strand rotational state, $(-120^\circ, 113^\circ)$. Renderings of the Fmoc-FF structure proposed by Smith et al.³⁵ were drawn in VMD using imported protein databank files received Andrew Smith.

CHAPTER 3. RESEARCH AIM: PEPTOID B28

3.1 Background and Introduction

3.1.1 Peptoid B28

The development of peptoid B28 was based on the self-complementary design motif of many self-assembling peptide systems.¹¹ In these systems, alternating hydrophobic and hydrophilic amino acid sidechains are sequestered on opposite “faces” of the molecule, which adopts a β -strand conformation.⁸ Consistent with this design motif, peptoid B28 contains 28 residues with alternating hydrophobic and hydrophilic sidechains. Counting from the amino terminus, the 14 even numbered residues in B28 are hydrophobic *N*-(2-phenylethyl)glycine units. The first 7 odd numbered sidechains are cationic (at neutral pH) *N*-(2-aminoethyl)glycine units, such that the first half of the B28 molecule would be considered a positively charged block. The odd numbered sidechains on the second half of the molecule are anionic *N*-(2-carboxyethyl)glycine units, resulting in a negatively charged block.³⁶ Peptoid B28 primary structure is shown in Figure 5. While peptide systems following similar design patterns very often adopt β -strand conformations, one of the primary driving forces behind assembly of β -sheet-rich amyloid fibers is believed to be intermolecular hydrogen bonding along the peptide backbones.³⁷ Because there are no amide hydrogen atoms in peptoids, backbone hydrogen bonding is not possible, thereby removing this as a contributor to self-assembly. Despite the lack of backbone hydrogen bonding capability however, peptoid B28 self-assembles into highly-stable nanosheets (see Figure 6) which are believed to be composed of molecules in extended “ Σ -strands”, a conformation analogous to a β -strand.^{11, 36} Furthermore, the organization of ionic

sidechains to produce like-charged blocks is believed to promote a brickwork-like intermolecular organization.³⁶ The alternating sequence motif of aromatic and ionic sidechains is quite general for nanosheet formation. This enables functionalization and structural engineering of nanosheets for a variety of applications including serving as affinity reagents, templates for the growth of composite materials, holding great potential for use as membranes for separations, and as a platform for chemical and biological sensing.¹⁴

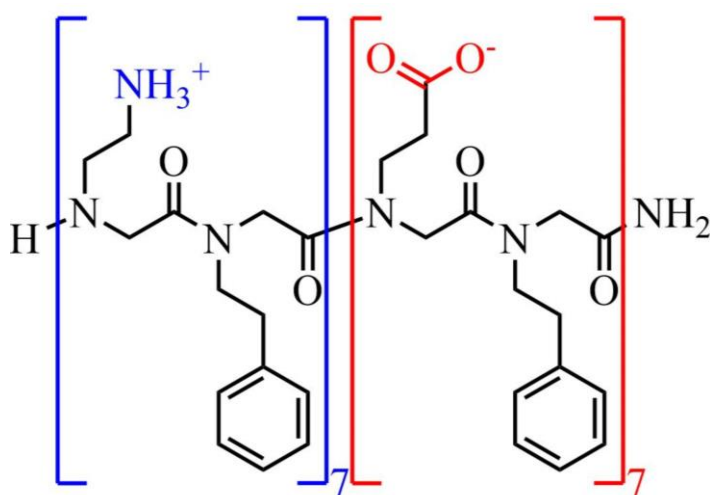


Figure 5 – Primary structure of peptoid B28 with the aminoethyl block in blue brackets and the carboxyethyl block in red brackets.

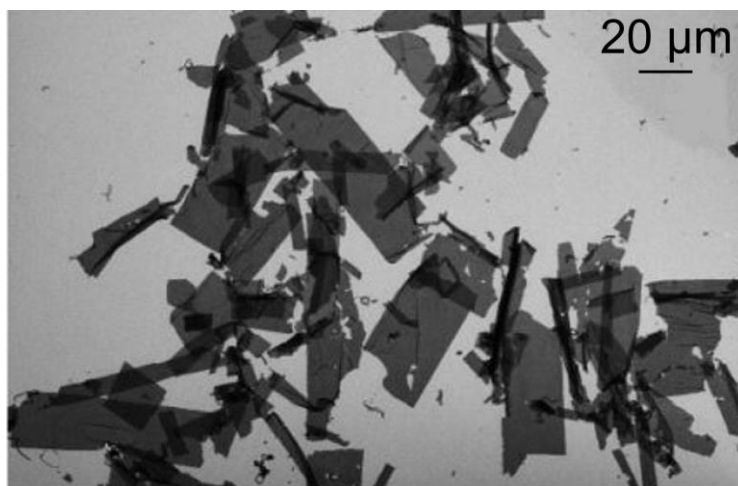


Figure 6 – TEM image of peptoid B28 nanosheets.

3.1.2 Previous Peptoid B28 Structural Measurements

Previous measurement techniques applied to peptoid nanosheets include aberration-corrected TEM, XRD, and AFM.^{11, 38} In the aberration-corrected TEM measurements, researchers identified what appear to be striations in the nanosheet assembly that are on the size-scale of individual peptoid molecules.¹¹ They appear to show monomers in extended conformations associating laterally with an approximate inter-strand distance of 4.5 Å.¹¹ This is useful information and provides a basis for assumptions made in an initial structural hypothesis,³⁶ but it does not provide the atomic-level resolution needed to test the accuracy of the hypothesized structure. XRD measurements show the same 4.5 Å value for inter-strand distances in peptoid nanosheets.³⁸ However, much like aberration-corrected TEM, the measurements do not provide the atomic-level resolution needed for structure determination. AFM measurements of peptoid nanosheets have been used to estimate the thickness of the nanosheet at 30 Å. Again, similar aberration-corrected

TEM and XRD, measurements of nanosheet dimensions are useful in formulating a structural hypothesis, but there is not enough detail to test the hypothesis.

In short, previous measurements of peptoid nanosheets provided information on the dimensions of a peptoid nanosheet that were critical the original proposed B28 nanosheet structure.³⁶ However, none of these techniques inform on the accuracy of the proposed structure at the molecular level. Solid-state NMR however, has been used extensively in probing atomic-level molecular structure in biological assemblies. This is why I believed solid-state NMR would be uniquely suited to complement the measurements already performed by delving past nanosheet dimensions and into the structural detail within the nanosheets.

3.1.3 Introduction to Research Aims

The overarching aim of my work with peptoid B28 was to use solid-state NMR to test a recently proposed molecular model of peptoid B28 nanosheets³⁶ and use molecular constraints obtained from solid-state NMR data to refine the model if necessary. To accomplish this goal we focused on a long-standing structural question regarding the configuration of backbone amide bonds (torsion angle ω) within peptoids. Double bond character at this site results in two possible values for ω . For peptides, *cis* amide bonds ($\omega = 0$) are rare and *trans* ($\omega = 180^\circ$) is the heavily favored configuration. For peptoids, theoretical calculations and solution NMR data suggest that *trans* remains the favored configuration, but the energy gap between *trans* and *cis* amide bonds (see Figure 7A and 7B) is reduced by the attachment of sidechains to backbone N atoms (peptide sidechains connect to $C\alpha$ atoms).^{34, 39} Thus, the theoretical calculations and solution NMR

measurements suggested that, despite the smaller energy gap, there would be no effect on backbone amide configurational distributions. However, no direct measurement of *cis/trans* isomerism in the backbone amide bonds of peptoids within a supramolecular assembly had yet been published.

In the same way that peptoid design was inspired by peptide primary structure, we looked to solid-state NMR as a high resolution analytical technique used to probe peptide molecular structure in supramolecular assemblies. Though no solid-state NMR studies of peptoid assemblies had yet been published, we hypothesized—based on standard sp^3 bonding orbitals and geometry—that C_{α} - C_{α} interatomic distance would vary sufficiently between the *cis* and *trans* configurations shown in Figure 7 such that we could probe the isomerization state using PITHIRDS-CT dipolar recoupling NMR. These experiments would simultaneously demonstrate the capability of solid-state NMR to probe molecular structure in peptoids as well as address long-standing concerns regarding peptoid backbone configurations.

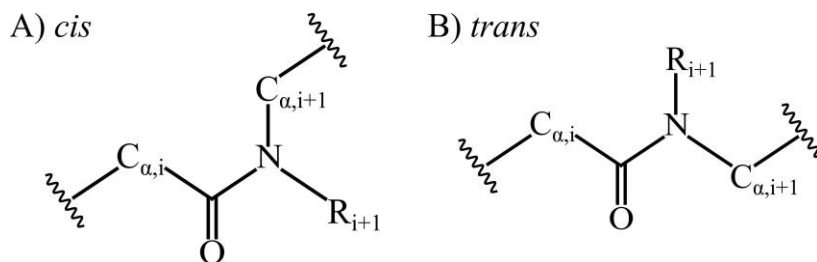


Figure 7 – Planar representations of peptoid backbone amide bonds in the *cis* (A) and *trans* (B) configurations.

3.2 Results and Discussion

3.2.1 Solid-State NMR

To begin the study, peptoid B28 samples were first produced unlabeled. Unlabeled peptoid B28 nanosheet samples were used to confirm that the material adopted the necessary ordered structure for successful application of more targeted and specific solid-state NMR measurements (see Figure 8). Following observation of an ordered molecular structure, further samples were synthesized with precise incorporation of ^{13}C isotopic labels at selected pairs of adjacent $\text{C}\alpha$ sites.

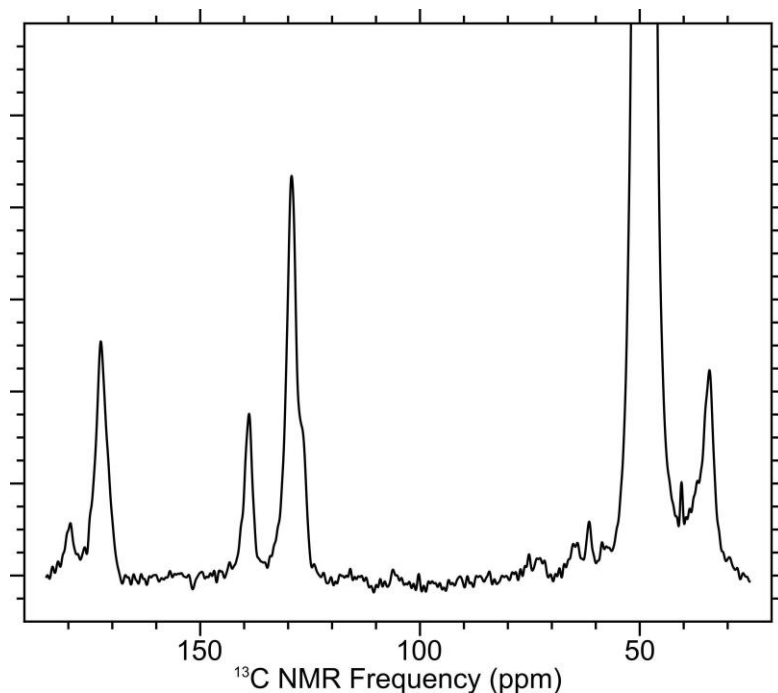


Figure 8 – CPMAS spectra of peptoid B28 nanosheets showing ^{13}C natural abundance signals corresponding to a well-ordered structure.

Though theoretical calculations and NMR of short peptoids in solution suggested little variation in backbone amide *cis/trans* isomerization, I still sought to test the hypothesis in the nanosheet assembly. To probe the isomerization state of B28 backbone amide bonds, I employed PITHIRDS-CT dipolar recoupling solid-state NMR on samples that were isotopically labeled with ^{13}C at pairs of adjacent $\text{C}\alpha$ sites. In tandem, molecular

dynamics simulations on single B28 Σ -strands were used to provide approximate interatomic distance distributions for adjacent $C\alpha$ sites in *cis* and *trans* configurations (Figure 9). Isomerization of the amide bond was expected to affect the distance between adjacent $C\alpha$ sites and therefore the strength of ^{13}C - ^{13}C magnetic dipolar couplings measured using PITHIRDS-CT.²⁹

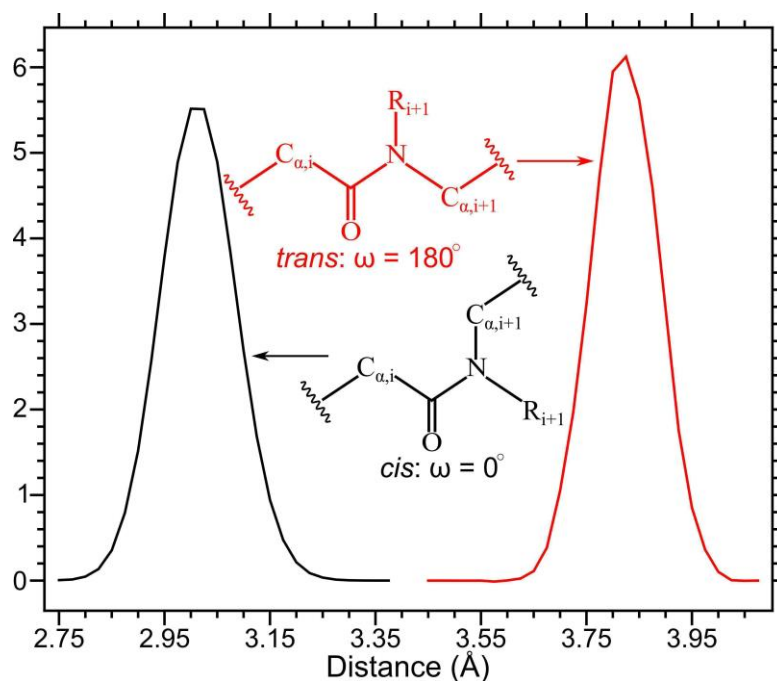


Figure 9 – Comparison of *cis* and *trans* configurations and their respective $C\alpha$ - $C\alpha$ distance distribution estimates from molecular dynamics simulations of peptoid B28 monomer units (single molecules).

From here, I examined the dependence of measured ^{13}C PITHIRDS-CT NMR peak intensity on ^{13}C - ^{13}C dipolar evolution time (Figure 10). Samples were ^{13}C -labeled at residues 6 and 7, 7 and 8, or 14 and 15 (see Figure 10A). For each ^{13}C labeled pair, experiments were performed on a nanosheet sample, and an unassembled, amorphous control sample for a total of 6 samples. The CPMAS NMR spectra of these samples are shown in Figures A5 of the Appendix. Each data point in Figure 10B and 10C represents

the integrated intensity of measured NMR signal for a specific evolution time under the influence of ^{13}C - ^{13}C magnetic dipolar coupling (estimated error based on NMR signal-to-noise is on the order of the symbol size). Data were corrected for the expected contribution of 1% naturally abundant ^{13}C background signal corresponding to unlabeled aliphatic sites in B28.

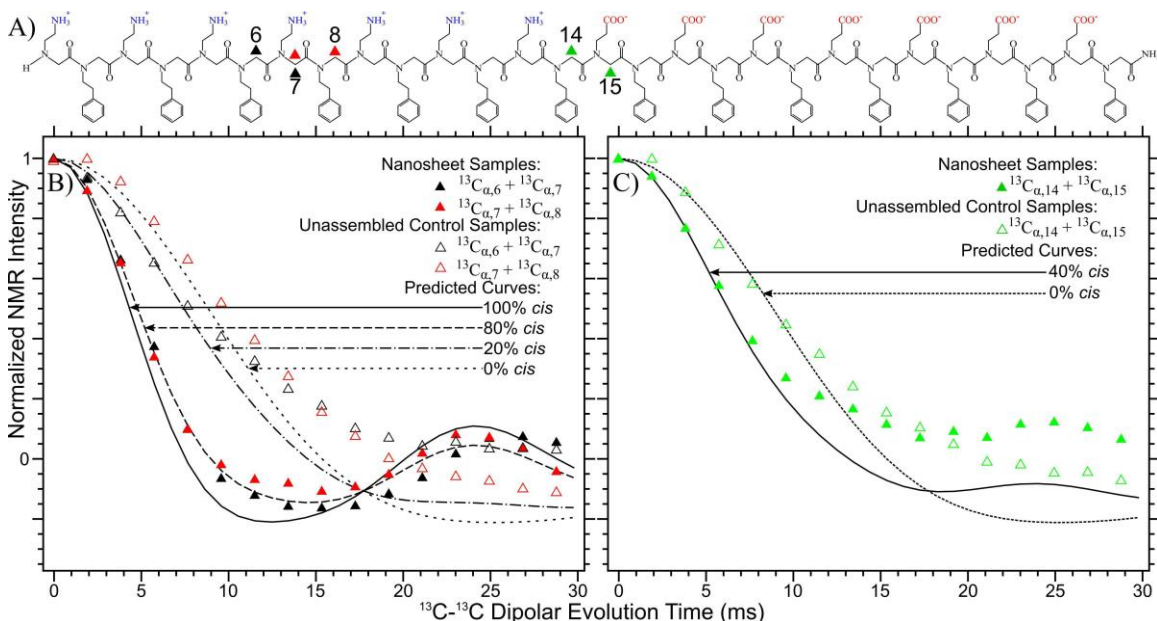


Figure 10 – A) Unabbreviated primary structure of peptoid B28 with ^{13}C -labeled C_α pairs identified by black triangles (6, 7), red triangles (7, 8), and green triangles (14, 15). B) PITHIRDS-CT data for C_α pairs (6, 7) and (7, 8). Nanosheet (*cis*) decays are indicated by filled triangles, and amorphous control (*trans*) decays are indicated by empty triangles. C) PITHIRDS-CT decays from nanosheet (filled triangles) and amorphous control samples (empty triangles) labeled at (14, 15). Color scheme for (B) and (C) is maintained from (A). Simulated curves are shown to indicate predicted PITHIRDS-CT decays for distance distributions corresponding to 100% *cis*, 80% *cis*, 20% *cis*, and 0% *cis* in (B) and 40% *cis*, and 0% *cis* in (C).

Nuclear spin simulations were performed using SPINEVOLUTIONTM in order to quantify the dependence of PITHIRDS-CT decay on interatomic distance for a pair of ^{13}C nuclei.³¹ The theoretical curves shown in Figure 10 are the sums of simulated NMR decays, weighted in terms of distributions of predicted ^{13}C - ^{13}C distances in Figure 9. All three

amorphous control samples exhibit similar decay curves (empty symbols in Figure 10B and 10C), indicative of a primarily *trans* amide bond population. In contrast, measured decays for nanosheet samples labeled at residues 6 and 7 and residues 7 and 8 (Figure 10B, filled symbols) are consistent with a predominantly *cis* configuration. Data from the nanosheet samples labeled at positions 14 and 15 (Figure 10C, filled symbols) indicate a more even split in the population with an estimated 40% contribution of the *cis* configuration. Potential effects of inter-molecular ^{13}C - ^{13}C dipolar couplings were considered using spin simulations (Figure A6) and we determined that the strongest possible intermolecular ^{13}C dipolar couplings would not affect our assessment of *trans* versus *cis* amide bonds.

The PITHIRDS-CT results in Figure 10 have important implications. Results for amorphous control samples are harmonious with previous experimental analyses on small, solvated peptoid molecules and theoretical predictions that suggest a lower energy for *trans* amide bonds.^{34, 39} However, here we experimentally observe, for the first time, that peptoid B28 nanosheets appear to exhibit significant contribution from the *cis* configuration at multiple backbone amide bonds. As we see it, our results motivate two possible explanations that are not necessarily mutually exclusive. First, that the energetics of intermolecular interactions occurring during self-assembly could be sufficiently strong to promote isomerization of amide bonds from *trans* to *cis*. Second, isomerization from *trans* to *cis* could occur prior to self-assembly. If this were true, it would likely indicate that the *cis* configuration increases the propensity for nanosheet assembly, given the results supporting *cis*-dominant nanosheets. Further studies would be required to experimentally characterize the influences of peptoid length, sidechain interactions, and nanoscale

assembly on amide bond isomerization. It is worth emphasizing that the sample preparation procedures for B28 nanosheet and amorphous control samples yield differing degrees of protonation in the hydrophilic sidechains which may impact chain conformation and propensity for amide bond isomerization.

3.2.2 Molecular Modelling

Until now, extended, linear molecular conformations in peptides and peptide-mimicking materials have always assumed an all-*trans* configuration along the backbone. Based on previous experimentation, we still believe B28 monomers adopt extended conformations within nanosheets.¹¹ As such, we simulated B28 monomers with the goal of determining whether or not an all-*cis*, low-energy state in which the molecule maintains overall linearity and sequestration of hydrophilic and hydrophobic sidechains is possible. The results indicate that this is indeed possible, and interestingly, that the correspondingly shorter molecular length of the “*cis* Σ -strand” would promote more compact arrangements of hydrophobic residues within nanosheet cores (see Figure 11).

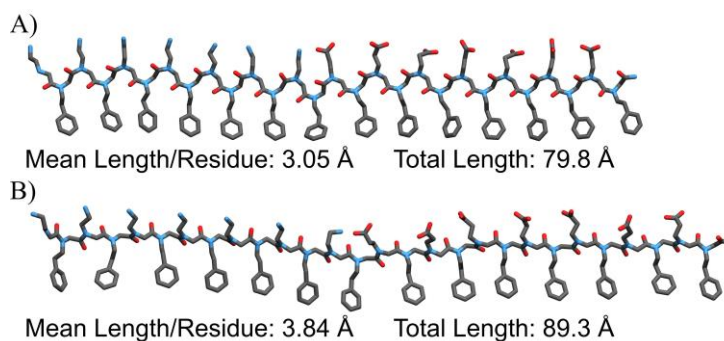


Figure 11 – A) *Cis* Σ -strand configuration. B) *Trans* Σ -strand configuration. Length/residue and total molecular length values were obtained through molecular dynamics simulation of peptoid nanosheets.

While the all-*cis* state of a B28 monomer is feasible according to molecular modeling simulation and quantum mechanical calculations, the same data also indicate that the all-*trans* monomer backbone features a lower, more energetically preferable folding scheme. While this finding is consistent with previous experimentation and simulation, it remained vexing given the PITHIRDS-CT data which clearly indicated *cis*-like interatomic distances between α -carbons in nanosheets. When the *cis* backbone configuration was introduced to nanosheet simulations, however, we found that though the *trans* state was favored for monomers in solution, the *cis* backbone yielded a lower energy minimum for the nanosheets as a whole. This is due in large part improved packing efficiency of the aromatic sidechains in the hydrophobic core afforded by the shorter molecular length of the extended *cis* backbone. What these simulations and calculations suggest is that when nanosheet assembly occurs, intermolecular interactions are able to overcome natural energetic barriers presented by intramolecular forces to produce configurations which would be unfavorable outside of a nanosheet (illustrated in Figure 12). This is both an illustration of the incredible difficulty inherent to careful designer self-assembly and accurate prediction of final molecular structure, as well as the information which may be gleaned from the effective combination of high resolution analytical techniques like solid-state NMR and the computing power of molecular dynamics simulations.

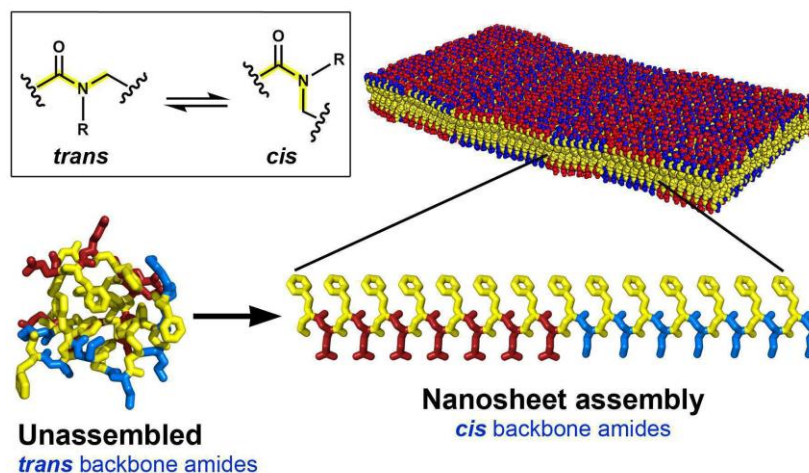


Figure 12 – Illustration showing the preference for *trans* in the unassembled state and *cis* in the nanosheet state.

To test our new *cis* nanosheet model we looked to residues 14 and 15 of peptoid B28. Recall that within nanosheets, PITHIRDS-CT data at this site appeared to show a near even distribution of *cis* and *trans* states. The spacing of the brickwork-like structure means that this site sits near a gap between two adjacent molecules. Application of umbrella sampling to the new model suggested that this site possessed a uniquely low free energy barrier for *cis*-to-*trans* isomerization. Further softening of the potential energy forcefields about the ω dihedral angle increased the isomerization rate at this site, leading to a near-even distribution of *cis* and *trans*. This behavior is consistent with the NMR data, providing further support for the *cis* model being a good approximation of the nanosheet structure observed by NMR. The final *cis* nanosheet model is shown in Figure 13 and the results of the umbrella sampling and forcefield softening are shown in Figure 14.

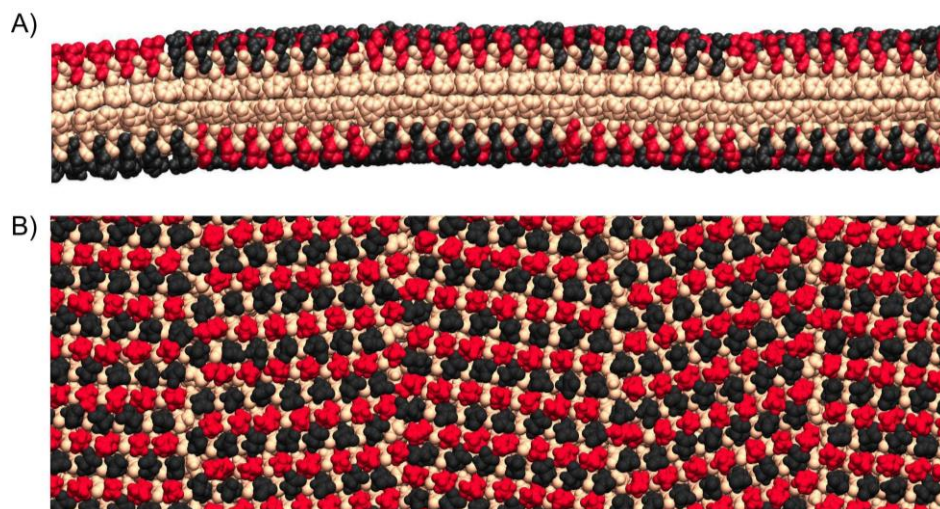


Figure 13 – A) Side-view and B) top view of new *cis* nanosheet model. N-(2-aminoethyl) residues are shown in red, N-(2-carboxyethyl) residues in black, and N-(2-phenylethyl) residues in black.

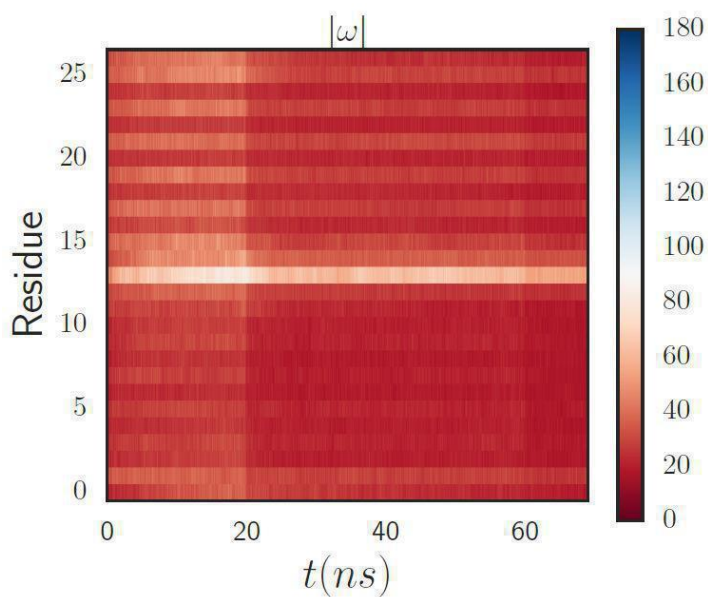


Figure 14 – Evolution of $|\omega|$ of each residue over all B28 chains in a biased simulation was an all-*cis* nanosheet. The middle residue shows a near equal distribution of *cis* and *trans*.

The addition of the *cis* backbone has also helped to rationalize other aspects of the nanosheets which had previously been unresolved. The dimensions of the *cis* nanosheet are

a better match for measurements taken using atomic force microscopy (AFM) and x-ray diffraction (XRD). Additionally, in introducing the *cis* backbone into the nanosheet structure, we found that this led to an overall energy reduction of $\sim 9k_B T$ ($5.3 \frac{kcal}{mol}$) per residue. This was due in large part to more efficient packing of phenylethyl sidechains in the hydrophobic core of the nanosheet. Therefore, our observation of *cis* amide bonds, combined with new modeling revelations, suggest that the proposed bilayer and brickwork arrangements are correct.

CHAPTER 4. RESEARCH AIM: FMOC-FF

4.1 Background and Introduction

4.1.1 *Fmoc-FF*

Fmoc-FF is one of the most commonly studied low molecular weight gelator systems.⁴⁰⁻⁴¹ It possesses only two amino acid residues (see primary structure in Figure 15), whereas most peptides which form stable hydrogels contain 8-16 amino acid residues.⁴² Study of *Fmoc-FF* began with research on pathological amyloid self-assembly, a hallmark of diseases such as Alzheimer's, Parkinson's, type II diabetes, and prion diseases.³ Researchers identified several peptide fragments from naturally occurring amyloid-forming peptides which could either self-assemble independently or inhibit self-assembly of their parent peptide. In each of these peptide fragments the researchers noted the presence of amino acids bearing aromatic sidechains. They also noted the significant impact of self-assembly behavior which often occurred with modification of the aromatic residues. This led researchers to the idea that π -stacking of aromatic side-chains was crucial to amyloid self-assembly.⁴³ Of particular interest was the Alzheimer's peptide, amyloid- β ($A\beta$), which features two adjacent phenylalanine residues at positions 19 and 20.⁴³ Because $A\beta$ fragments containing the FF motif were found to either self-assemble independently or inhibit $A\beta$ self-assembly, researchers sought to isolate the FF motif. In pursuing this, Reches and Gazit demonstrated the capability of FF to self-assemble into rigid nanotubes⁴⁴, a phenomenon which had been shown a few years prior to their report.⁴⁵ Reches and Gazit continued their work on the FF system by modifying the N- and C-termini to probe the effect of electrostatic interaction on FF self-assembly. They showed that the addition of an

Fmoc group at the N-terminus lead to formation of hydrogels supported by nanofibers with amyloid-like morphology and significantly smaller diameters than the FF nanotubular arrays.¹⁰ Fmoc-FF hydrogels have since become a prominent model system in development of LWMG applications.

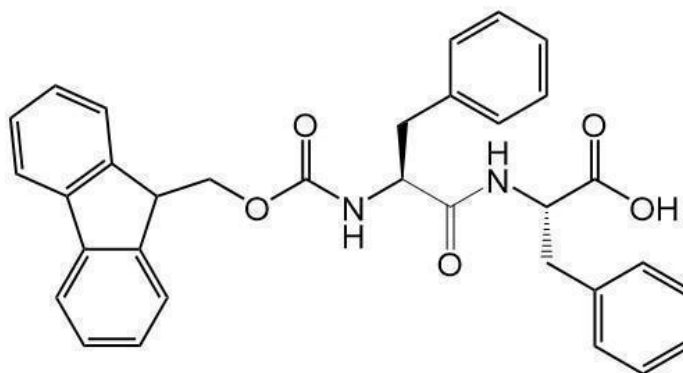


Figure 15 – Primary Structure of Fmoc-FF.

In addition to applications development, Fmoc-FF has also been shown to exhibit curious thermodynamic behavior. In peptide self-assembly, assembled structure—particularly amyloids—are very stable. Breaking these structures down over observable time-scales typically involves introducing a new variable, such as heat, to induce denaturation of the assembly. Diluting the peptide system below its critical assembly concentration will very often lead to no measureable change in peptide assemblies. Although it's still worth pointing that the slow, inexorable march of thermodynamics will ultimately lead to breakdown of assembled structure over time-scales outside the limits of laboratory observation. In contrast, Fmoc-FF hydrogels show measureable reversibility of assembly in response to changes in solvent composition and Fmoc-FF concentration.⁴⁶ Colloid scientists—including our partners for much of this Fmoc-FF research project, Nikola Dudukovic and his PhD advisor Charles Zukoski—have surmised that the observed

equilibrium behavior would enable accurate plotting of Fmoc-FF phase diagrams analogous to colloidal phase diagrams.⁴⁰

4.1.2 Previous Fmoc-FF Structural Measurements

Structural measurements of Fmoc-FF have consisted almost entirely of probing for peptide secondary structure using FTIR and CD spectroscopy. Circular dichroism is a commonly used method of exploiting optically active molecules with chiral centres. For peptides, CD absorption spectra are sensitive to secondary structure.⁴⁷ In the case of Fmoc-FF, CD measurements have used to conclude that assemblies exhibit β -sheet secondary structure.^{35, 48} The measurements do indeed exhibit classical β -sheet absorbance, but there is no precedent for the effect of the Fmoc group on absorbance profile. I do not believe it is wise to make interpretation of Fmoc-FF secondary structure based on standards established for peptide secondary structure.

The more thorough structural studies of Fmoc-FF have relied more heavily on FTIR measurements than on CD.^{35, 49} The problem is that they are divided on their conclusions. Each study produced a reasonable molecular model, but one concluded that Fmoc-FF nanofibers form a well-ordered assembly composed of Fmoc-FF molecules arranged anti-parallel to one another³⁵ and the other concluded that the assemblies were disordered in the FF subunit.⁴⁹ Furthermore, other studies have provided FTIR data and analysis for Fmoc-FF assemblies, each of which conclude that Fmoc-FF assemblies form anti-parallel β -sheets.^{16, 18, 21} The conclusions are based on absorbance of the amide I band, which in FTIR spectra appears in the 1700-1600 cm^{-1} wavenumber range.⁵⁰ For β -sheet secondary structure in peptides, the amide I stretch should appear in the 1638-1632 cm^{-1} range. If it

is an anti-parallel β -sheet, there should be an additional signal in the 1695-1675 cm^{-1} range.⁵⁰ The problem here is that in each of the studies which concluded an Fmoc-FF anti-parallel β -sheet, the amide I stretch ranges 1650-1625 cm^{-1} .^{16, 18, 21, 35} In the study that posited a disordered structure, the amide I stretch was 1645 cm^{-1} .⁴⁹ The divergent FTIR data are summarized in Figure A8 and A9 of the appendix. Additionally, while each of the FTIR studies referenced so far exhibits the anti-parallel signal at 1695-1675 cm^{-1} , this has been called into question as well. In a study assessing the viability of FTIR as a means of assigning secondary structure in Fmoc-FF, researchers were able to show that removing the carbamate group from the Fmoc portion of the molecule eliminated the canonical anti-parallel β -sheet signal from the FTIR spectra.⁵¹

To summarize, the most prominent method of assessing structure in Fmoc-FF systems, FTIR, appears highly subject to individual interpretation, with very similar results being given highly divergent interpretations. Additionally, there is uncertainty as to whether or not standard peptide secondary structure assignments from FTIR may be applied directly to Fmoc-FF because of the contribution from the Fmoc group.

Because of the controversy surrounding FTIR interpretation in Fmoc-FF assemblies, I do not believe it is a good way of assessing structure in these systems. Meanwhile, solid-state NMR provides atomic-level structural detail based on the local electronic environment on magnetically susceptible nuclei. This means solid-state NMR gives information directly on the arrangement of atoms in the sample and is far less subject to individual interpretation. This makes solid-state NMR far superior to both FTIR and CD as a technique for probing structure in Fmoc-FF assemblies.

4.1.3 Introduction to Research Aims

My work with Fmoc-FF began with questions surrounding variability of Fmoc-FF nanofiber morphology when self-assembly solvent environment was varied. Together with Nikola Dudukovic and Charles Zukoski of the University of Illinois in Urbana, Champagne we were able to show this variability using confocal microscopy and transmission electron microscopy (Figure 16). Morphological variation of nanofibers is a known property of A β specifically⁵² and amyloid forming peptides in a more general sense.⁵³

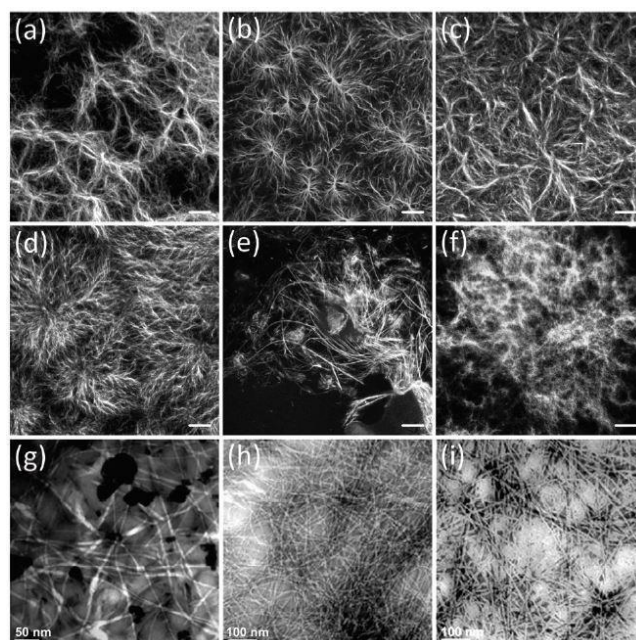


Figure 16 – (A-F) Confocal microscopy images of Fmoc-FF gels in: A) DMSO/H₂O, B) acetone/H₂O, C) methanol/H₂O, D) HFIP/H₂O, E) benzene, and F) toluene. Scale bars represent 10 μm. (G-I) TEM images of Fmoc-FF gels in G) DMSO/H₂O, H) methanol/H₂O, and I) toluene.

Observation of these amyloid-like properties in Fmoc-FF assemblies led us to two primary questions: 1) ‘Are Fmoc-FF nanofiber structures well-ordered at the molecular level?’ and 2) ‘What is the level of accuracy in two previously proposed, non-harmonious

Fmoc-FF modeling schemes?’^{35, 49} The first molecular model, proposed by Smith et al., used potential energy minimization to generate a tubular fiber structure composed of Fmoc-FF molecules arranged anti-parallel to one another and in a helical pattern along the length of the fiber.³⁵ The model is supported experimentally by FTIR and CD measurements, the results of which have been interpreted to suggest the presence of anti-parallel β -sheets and β -sheets, respectively. Multiple subsequent studies have used FTIR and CD in an attempt to characterize Fmoc-FF nanofiber secondary structure and reached similar conclusions regarding β -sheet-like secondary structure.^{48, 54} It’s also worth noting, however, the presence of the Fmoc group has caused some researchers to question the conclusions reached through interpretation of FTIR data.⁵¹ The second model posits a micelle-like structure in which the nanofiber core is stabilized by π -stacking of the Fmoc groups in the ‘hydrophobic’ portion of the micelle, with the amino acid sidechains adopting disordered conformations on the ‘hydrophilic’ surface of the micelle.⁴⁹

My aim here is to show that well-established solid-state NMR techniques for peptide structure determination may be successfully translated Fmoc-FF systems in order to address these questions.

4.2 Results and Discussion

4.2.1 Solid-State NMR

4.2.1.1 CPMAS

In addressing questions regarding overall order of Fmoc-FF assemblies, I used CPMAS to probe Fmoc-FF nanofibers formed in 5% DMSO, 5% methanol, 80% methanol,

and toluene. The results of these experiments are shown in Figure 17. Additionally, at this time I ran CPMAS on a sample of Fmoc-FF with uniform ^{13}C labeling on the phenylalanine residues to differentiate between amino acid and Fmoc signals, results of which are shown in Figure A7 of the appendix.

These solvent environments were chosen because Fmoc-FF nanofibers self-assemble in each environment, imaging techniques are able to show clear morphological variation in those fibers, and the chosen solvents represent widely varying degrees of polarity, hydrogen bonding capability, and dispersive forces. In particular, assembly of nanofibers in toluene was quite surprising. First, given the hydrophobicity and aromaticity of toluene, self-assembly of Fmoc-FF seemed unlikely because it is believed to be initiated by hydrophobic collapse and stabilized by π -stacking of the Fmoc groups and phenylalanine sidechains. Additionally, we have the proposition that solvent-bridged hydrogen bonding is crucial to dipeptide self-assembly.⁵⁵ Toluene, however, has very little hydrogen bonding capability.

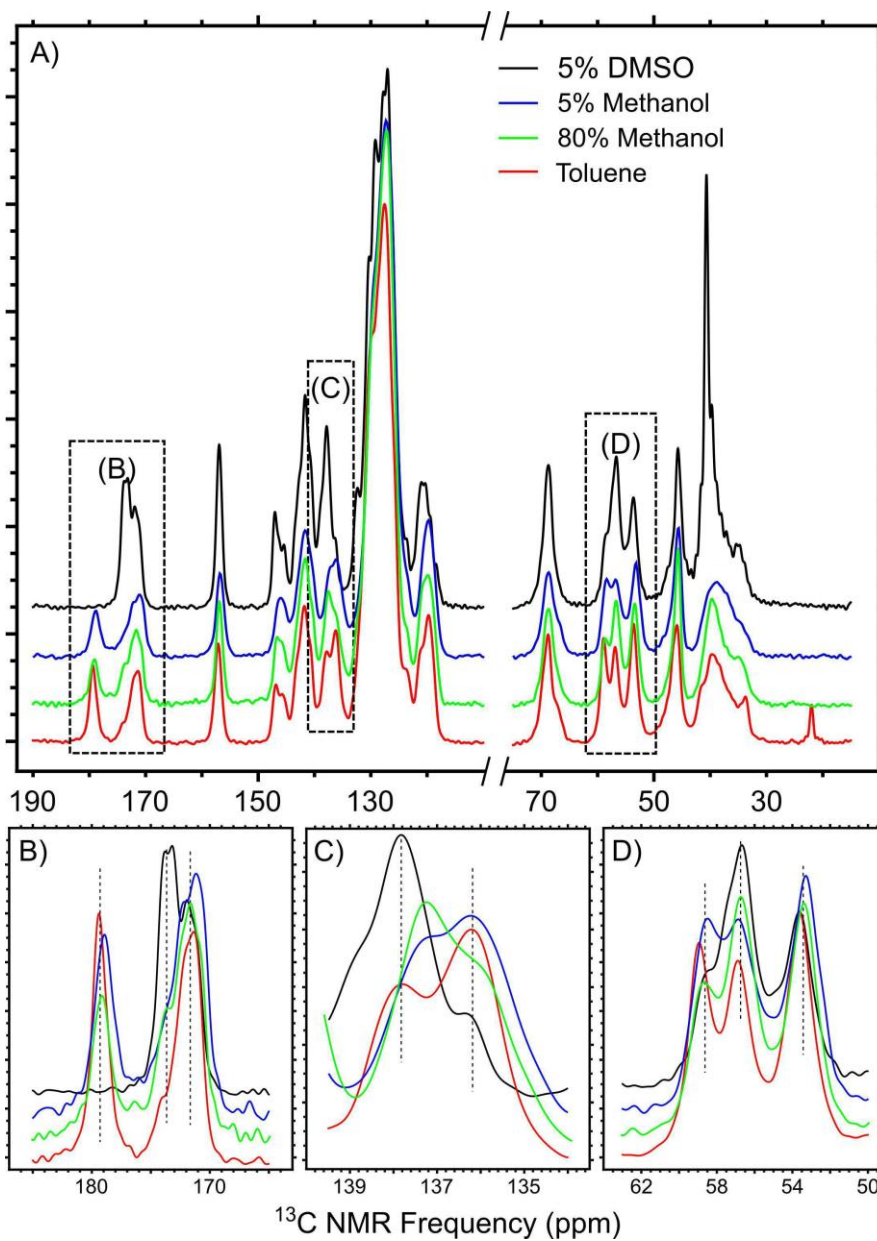


Figure 17 – A) CPMAS spectra obtained from Fmoc-FF nanofibers self-assembled in 5% DMSO (black), 5% methanol (blue), 80% methanol (green), and toluene (red). B) carbonyl, C) γ -carbon, and D) α -carbon signals from each spectrum.

The sharp line-widths of each of the spectra shown in Figure 17 are indicative of ordered molecular structure within the samples. Additionally, the CPMAS data show substantial variation in chemical shift across the different solvent systems in areas known to be sensitive to structural change in peptide systems, pointing to structural polymorphism.

Figure 17B shows the carbonyl region of Figure 17A, in which there are two significant peaks in each spectrum due to the carbonyl groups of the phenylalanine residues. From the DMSO sample, we see two peaks at about 172.5 and 174 ppm (phenylalanine carbonyl signals)^{1, 56} corresponding to chemical shift values of protonated carboxylic acids. However, in both methanol samples and the toluene sample, there is a clear shift in one peak from 174 to 179 ppm. A shift of this magnitude is consistent with deprotonation of the C-terminus of the molecule.⁵⁶

Peak shifting behavior can be seen in the aromatic and aliphatic regions of the spectra as well. Figure 17C shows the signal between 135 and 139 ppm in each spectrum, corresponding to the γ -carbons of the two phenylalanine residues, the only aromatic carbon atoms capable of substantial conformational variation.^{1, 56} Each spectrum has a peak at about 136 ppm, but intensity varies across each solvent. The second peak in each spectrum is of variable intensity and falls between 137 and 138 ppm. In this peak however, the position is shifted slightly up-field in the methanol samples compared to the DMSO and toluene samples.

Figure 17D shows the α -carbon signals of the phenylalanine residues, which fall in the 53-59 ppm range.^{1, 56} Moving downward from DMSO to toluene in Figure 17D, we can see the clear transition and growth of a third peak which appears in the DMSO spectrum as only a small “shoulder” on the large peak near 57 ppm. Also, unlike in Figures 17B and 17C, we see three significant signals. This suggests a significant contribution from three α -carbon conformational populations, where the fraction of each is dependent on the solvent environment of gelation. This would in turn indicate the presence of multiple distinct and well-ordered molecular conformations within these gels.

Finally, the β -carbon region of the spectrum—about 33-34 ppm—is less intense and more broad than in the regions highlighted in Figure 17B-D.^{1,56} The decreased intensity and increased broadness of the signals here indicate that the β -carbons adopt less-ordered conformations than the regions highlighted in Figure 17B-D, suggesting they may not be critically involved in self-assembly. Standing out starkly from this interpretation is a very sharp peak in the DMSO spectrum at about 38 ppm. I believe this signal originates in part from residual DMSO remaining in the sample.⁵⁶ Recall that a previous study has proposed that solvent-bridged hydrogen bonding is crucial to dipeptide nanofiber formation,⁵⁵ and DMSO is capable of participating as a hydrogen bond acceptor. However, there is no evidence to suggest the incorporation of DMSO into fiber structure, and formation of Fmoc-FF nanofibers in toluene suggests solvent-bridged hydrogen bonding is not required for Fmoc-FF nanofiber self-assembly.

4.2.1.2 Two-Dimensional CHHC and fpRFDR NMR

With the observation of an ordered molecular structure in each of these systems via CPMAS, I had shown that Fmoc-FF assemblies were observable through NMR. With this in mind I moved to the proposed molecular models.^{35, 49} First, the prediction by Mu and coworkers that the amino acid sidechain portion of the molecule adopts a disordered conformation is inconsistent with each of the CPMAS data sets shown in Figure 17.

From here I moved to a molecular model proposed by Smith et al. in 2008. Using the 2D NMR experiments, CHHC and fpRFDR, I probed Fmoc-FF nanofiber samples containing 100% ¹³C-labeled phenylalanine residues for anti-parallel β -sheet molecular contacts. The results of these experiments are shown in Figures 18-21. For the sample

assembled in 5% methanol, I increased the methanol volume fraction to 10% in order to simplify sample preparation. CPMAS data indicate no change in molecular structure between the two samples. In each fpRFDR spectrum, the data shows no interaction amongst signals in the 53-59 ppm region, indicating none of the signals originate from directly bonded pairs of atoms. However, all fpRFDR spectra show interaction between signals in the 53-59 ppm region with signals in the 33-43 ppm region (green circles). This is the expected interaction between α -carbon (red circles) and β -carbon signals (orange circles). Unlike the fpRFDR data, the CHHC data show unambiguous dipolar coupling between signals in the 53-59 ppm region (blue circles). In order for this signal to appear, there must be magnetization transfer following the pattern previously described for CHHC. We also see CHHC contacts between α -carbon and β -carbon signals, the expected interaction between directly bonded α -carbon and β -carbon atoms. One-dimensional 'slices' from each of the CHHC and fpRFDR spectra are shown in Figure 22. The slices show the relative cross-peak intensities from CHHC and fpRFDR and absence of α - α interaction in the fpRFDR data. Finally, mapping of the α -carbon and carbonyl signals in the fpRFDR indicate that we are seeing CHHC contacts between F1 and F2 of the FF subunit (results shown in Figure A10 of the appendix).

To ensure that the observed CHHC contacts are not the result of intramolecular interactions, we prepared a 50% isotopically diluted of Fmoc-FF nanofiber sample for CHHC and fpRFDR (Figure 23). The results show a decrease in signal intensity of α - α interactions relative to the individual α -carbon signals. This indicates the α - α interaction signals we are observing are originating from intermolecular contacts.

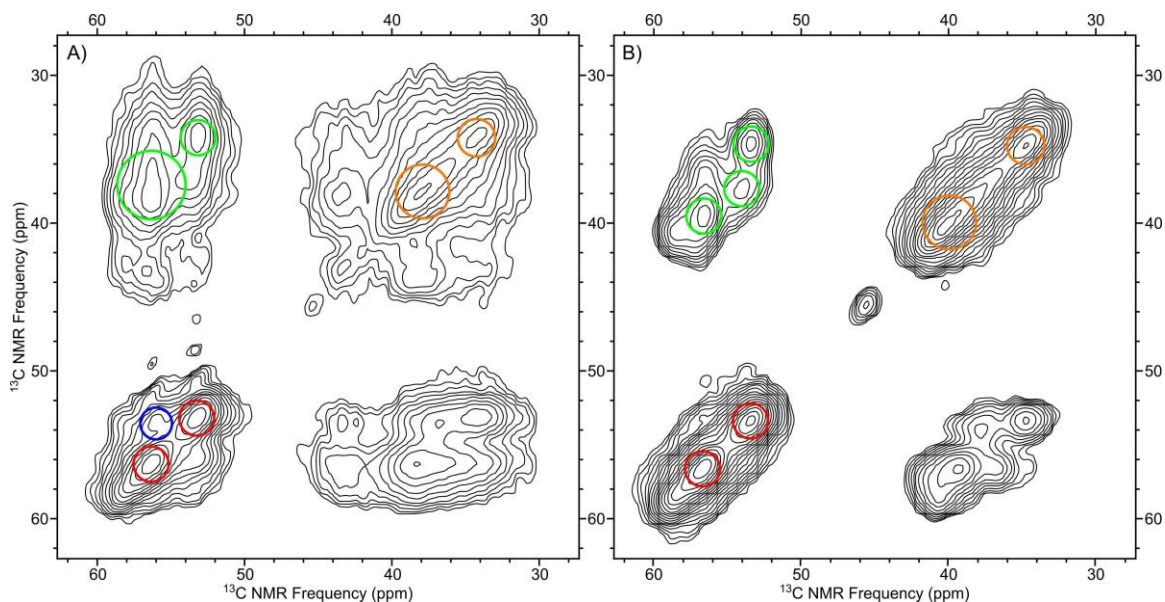


Figure 18 – Side-by-side comparison of CHHC (A) and fpRFDR (B) spectra for Fmoc-FF nanofibers assembled in 5% DMSO. Red circles highlight α -carbon signals, orange circles show β -carbon signals, blue circles show α - α correlation signals, and green circles show α - β correlation signals. Correlation signals are mirrored on each side of the diagonal containing α -carbon and β -carbon signals.

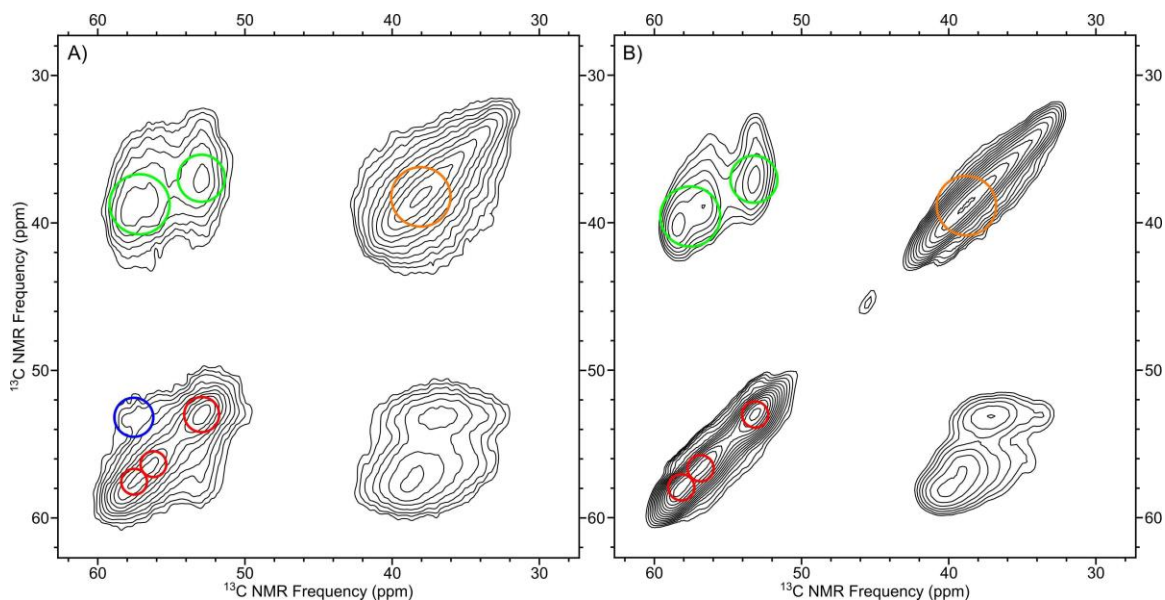


Figure 19 – Side-by-side comparison of CHHC (A) and fpRFDR (B) spectra for Fmoc-FF nanofibers assembled in 10% methanol. Red circles highlight α -carbon signals, orange circles show β -carbon signals, blue circles show α - α correlation signals, and green circles show α - β correlation signals. Correlation signals are mirrored on each side of the diagonal containing α -carbon and β -carbon signals.

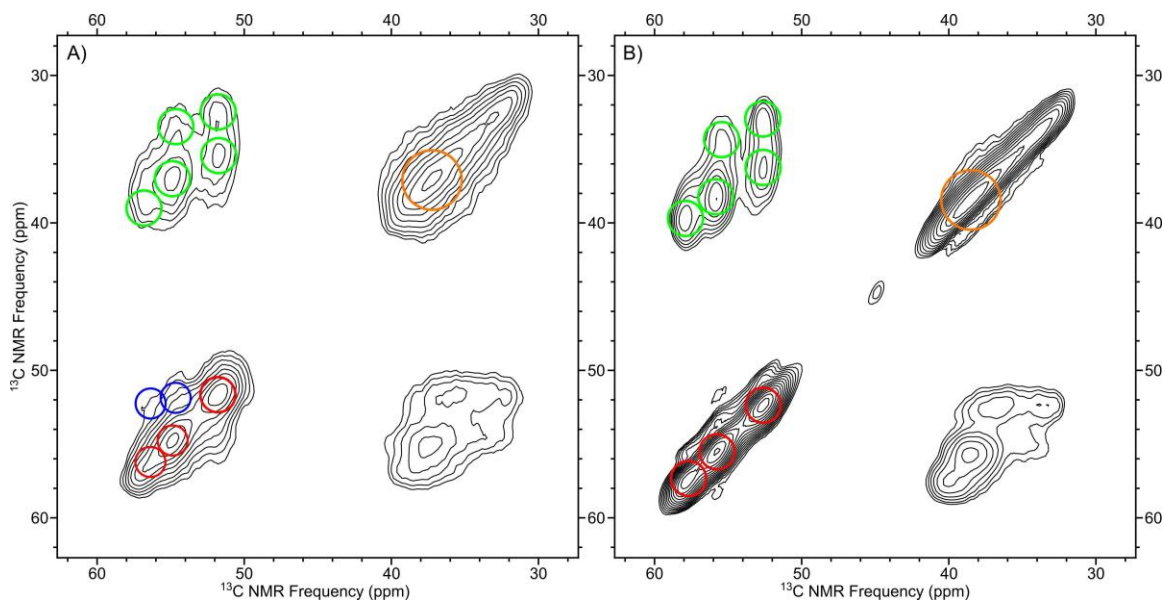


Figure 20 – Side-by-side comparison of CHHC (A) and fpRFDR (B) spectra for Fmoc-FF nanofibers assembled in 80% methanol. Red circles highlight α -carbon signals, orange circles show β -carbon signals, blue circles show α - α correlation signals, and green circles show α - β correlation signals. Correlation signals are mirrored on each side of the diagonal containing α -carbon and β -carbon signals.

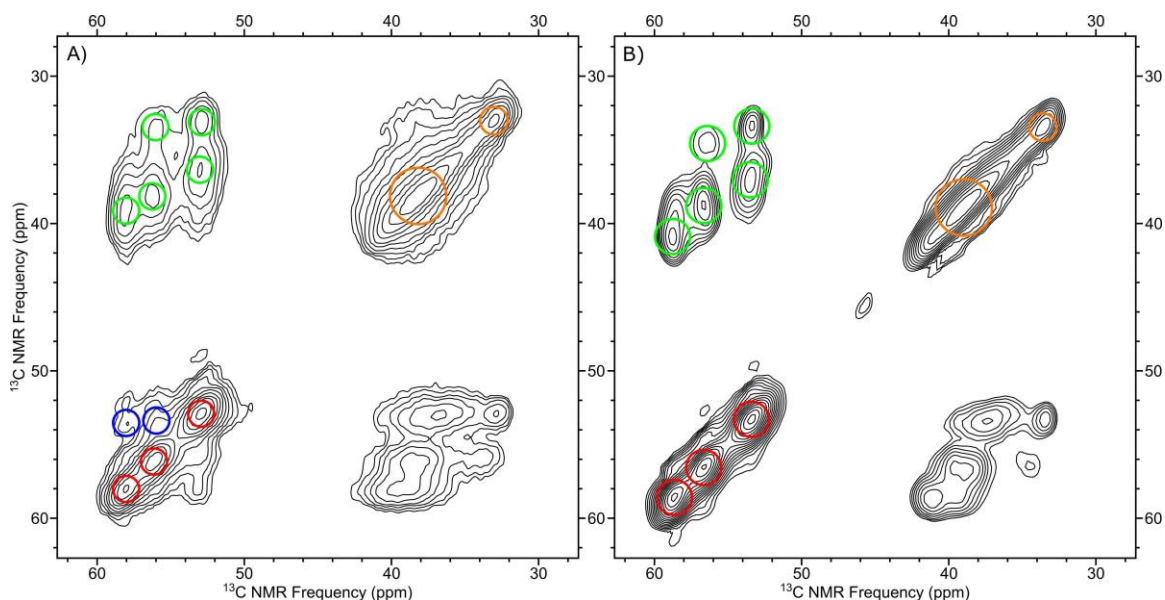


Figure 21 – Side-by-side comparison of CHHC (A) and fpRFDR (B) spectra for Fmoc-FF nanofibers assembled in toluene. Red circles highlight α -carbon signals, orange circles show β -carbon signals, blue circles show α - α correlation signals, and green circles show α - β correlation signals. Correlation signals are mirrored on each side of the diagonal containing α -carbon and β -carbon signals.

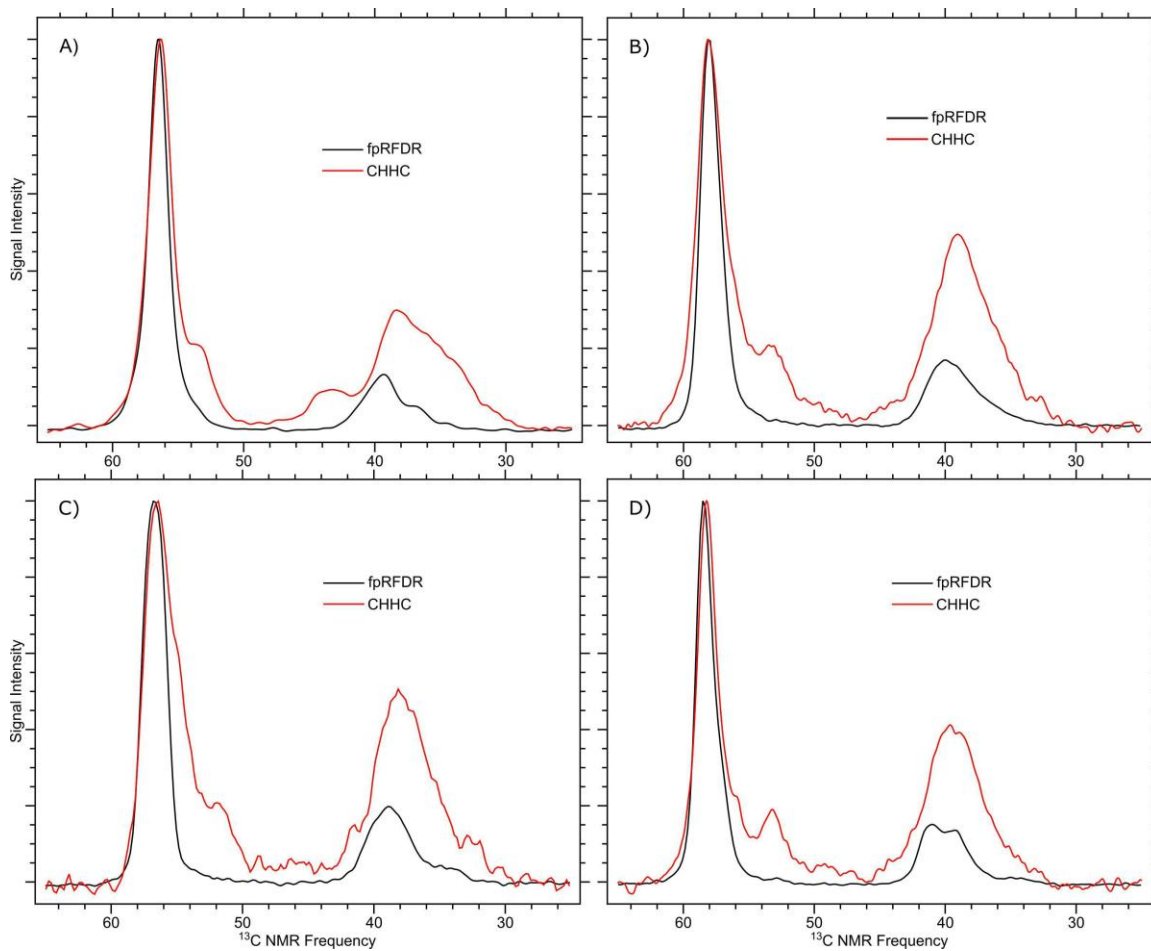


Figure 22 – Overlay of one-dimensional CHHC and fpRFDR slices at 58 ppm from samples in A) 5% DMSO, B) 10% methanol, C) 80% methanol, and D) toluene.

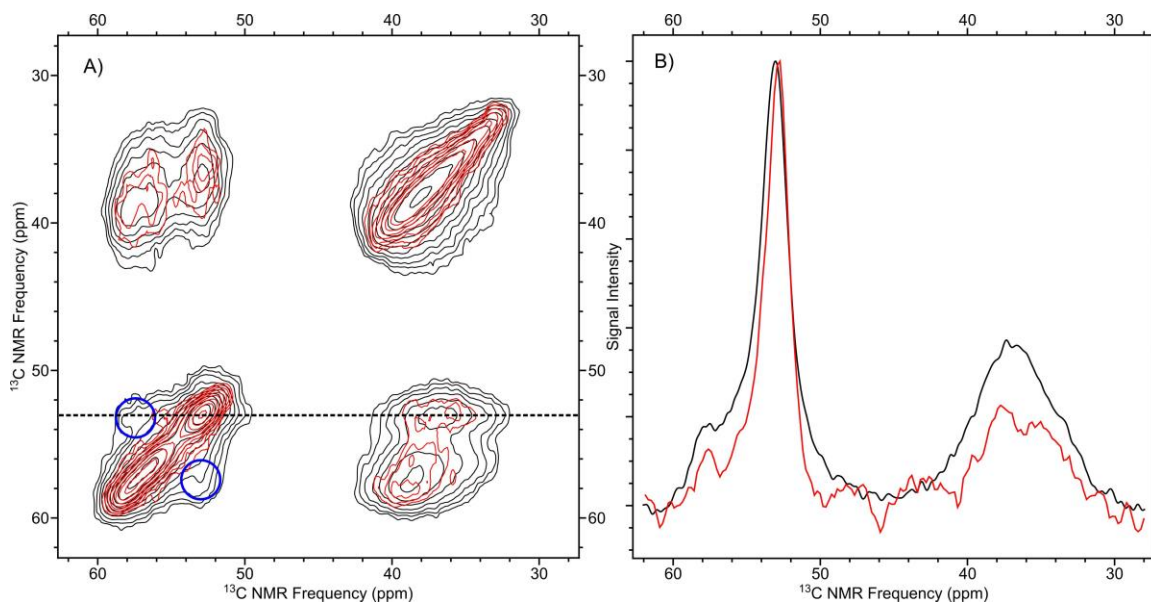


Figure 23 – A) Overlay of CHHC spectra from Fmoc-FF formed in 10% methanol using 100% ^{13}C -labeled material (black) and 50/50 ^{13}C labeled/unlabeled (red). B) One-dimensional slice comparison at ~53 ppm from both spectra in (A).

4.2.2 Molecular Modeling

To rationalize the two-dimensional NMR data shown in the previous section, I turned to molecular modeling using VMD. First, I reached out to Rein Ulijn and Andrew Smith to acquire a copy of their proposed model. Analysis of this model showed that though the structure predicted an anti-parallel backbone arrangement, it was not consistent with the CHHC NMR data.

Moving forward, we sought to rationalize the NMR data by using idealized molecular structures. Based on the forces involved in maintaining β -sheet secondary structure in peptides and on the results of a recent study which substituted peptoid residues for phenylalanine residues in Fmoc-FF,⁵⁷ we believed backbone hydrogen bonding was critical. We then generated diphenylalanine backbone arrays which would present favorable hydrogen-bonding sites and checked these structures for arrangements which

would give the contacts observed using CHHC NMR. Figure 23 shows our three most reasonable backbone arrays in terms of backbone hydrogen bonding availability: parallel, antiparallel, and an antiparallel flipped arrangement, alongside the arrangement predicted by Smith et al.

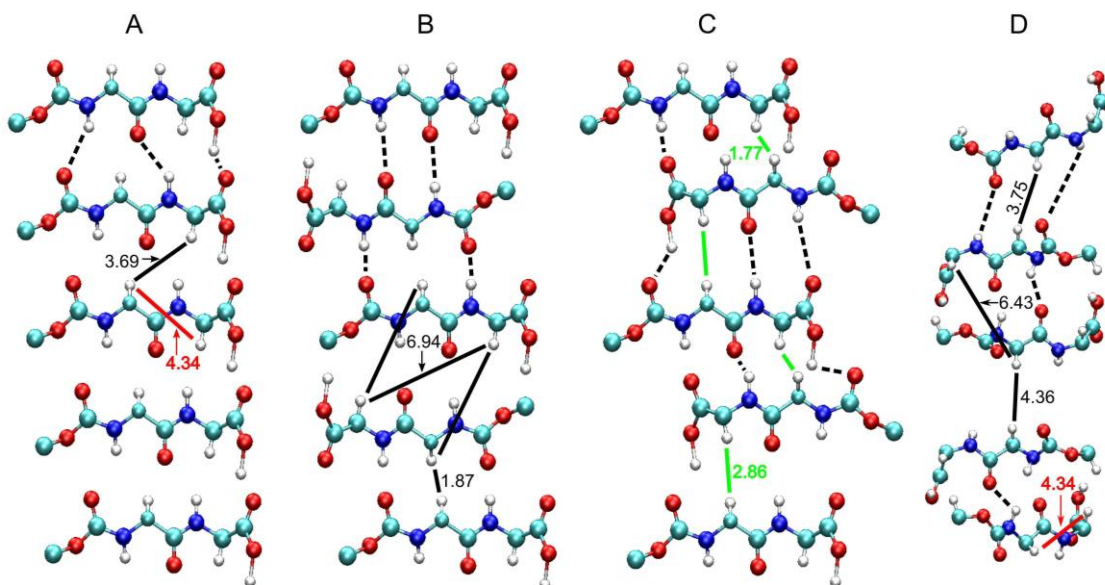


Figure 24 – A) Idealized, parallel diphenylalanine backbone, B) Idealized, antiparallel diphenylalanine backbone, C) Idealized, flipped antiparallel diphenylalanine backbone, and D) Smith diphenylalanine backbone. Dashed lines indicate hydrogen bonds, solid black lines indicate intermolecular $H\alpha$ pairs outside CHHC detection range, red lines indicate intramolecular $H\alpha$ pairs, and green lines indicate intermolecular $H\alpha$ pairs inside CHHC detection range. All distances are given in angstroms (\AA).

In Figure 23 shows that though there are multiple possible hydrogen bonding alignments, only one alignment—flipped antiparallel—also predicts an arrangement consistent with the NMR data. Most interestingly, despite the fact that we evidence of significant polymorphism in both microscopy and CPMAS NMR data, CHHC appears to indicate that this flipped anti-parallel arrangement is common to all Fmoc-FF assemblies

tested. This study includes samples assembled using heating to induce dissolution (toluene), solvent switch (5% DMSO), and both heating and solvent switch (methanol gels). Additionally, the study which highlighted the importance of backbone hydrogen bonding using peptoid substitution studied Fmoc-FF hydrogels formed using a solvent switch method with DMSO and a pH switch,⁵⁷ so it appears that assemblies formed using the pH switch and solvent switch methods rely similarly on backbone hydrogen bonding. It is highly possible then that the flipped antiparallel hydrogen bonding pattern identified here is present in assemblies formed using the pH switch method as well.

4.2.3 FTIR

Because this study marks the first use of solid-state NMR to study Fmoc-FF assemblies, I sought connect this work to previous studies of Fmoc-FF. Up to the present, determination of antiparallel β -sheet-like structure in Fmoc-FF assemblies has been based on interpretation of FTIR.^{16, 35, 54} I ran FTIR on hydrogels from each of the four solvents from the CHHC and fpRFDR experiments. Results are shown in Figure 24. In each system we see signals previously attributed to an anti-parallel β -sheet-like arrangement in Fmoc-FF systems: a large peak around $\sim 1640\text{-}1650\text{ cm}^{-1}$ and a smaller peak around $\sim 1690\text{-}1700\text{ cm}^{-1}$.¹⁶ The signals vary slightly from solvent to solvent, with peaks broadening or shifting slightly. Dashed lines in the figure show the range for the large peak around $\sim 1640\text{-}1650\text{ cm}^{-1}$, dotted lines show the range for the smaller peak around $\sim 1690\text{-}1700\text{ cm}^{-1}$, and a single dash-dotted line shows a small “shoulder” signal which appears in the DMSO, 10% methanol, and 80% methanol gels.

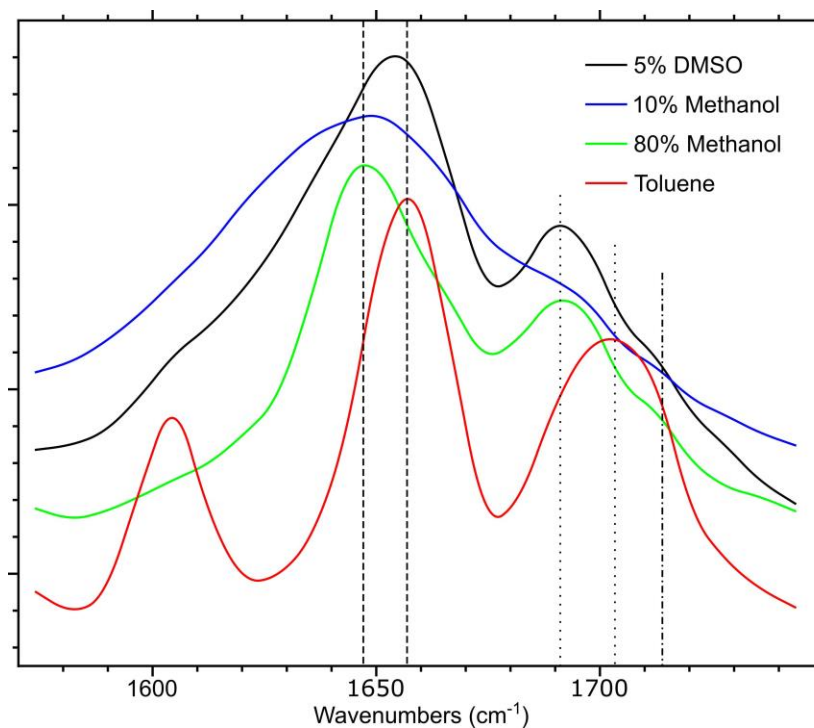


Figure 25 – FTIR spectra from Fmoc-FF formed in 5% DMSO (black), 10% methanol (blue), 80% methanol (green), and toluene (red).

Though FTIR has been a common tool used in assessing Fmoc-FF secondary structure, there are a few points of interest that are worth noting. First, the peak attributed to a β -sheet signal is sometimes near 1650 cm^{-1} . A peak in this region is often attributed to disorder in a peptide system,⁴⁹ though from NMR we know that this is not the case for these Fmoc-FF systems. Additionally, the peak near 1690 cm^{-1} attributed to anti-parallel β -sheet structure has been shown to disappear if the carbamate portion of the Fmoc group is removed.⁵¹ It is not clear if that is because the peak at 1690 cm^{-1} is solely from the carbamate stretch or if removal of the carbamate group has an effect on assembled structure. Recall though, that despite the uncertainties of FTIR measurements of Fmoc-FF, NMR appears to validate previously drawn conclusions.

Finally, each spectrum appears to exhibit some signal near 1600 cm^{-1} . It is not clear at this stage what aspect of the system is causing the absorbance at this point. It has been shown in the past that labeling with ^{13}C in larger peptides can result in amide I shifts to this region of the spectrum, but this is like not the case here.⁵⁰ Each of the FTIR samples were produced using unlabeled material, meaning that any ^{13}C interference would have to come from natural abundance ^{13}C . There is no evidence to suggest this is occurring. Small signals in this region can be seen in some of the FTIR measurements referenced previously, though it did not appear to be significant to the authors.^{18, 21}

CHAPTER 5. CONCLUSIONS AND FUTURE WORK

5.1 Peptoid B28

The NMR data presented here show evidence of site-dependent, assembly-driven *trans*-to-*cis* isomerization in the backbone amide bonds of peptoid B28 nanosheets. The measurements led to development of a new molecular model more closely aligned with NMR, AFM, and XRD measurements than the previous model.³⁶

Where does the work go from here? With specific regard to peptoid B28, there remain aspects of the new molecular model that have not been confirmed experimentally. First is the brickwork arrangement of molecules within the nanosheet. There is strong indirect evidence in the modeling and dipolar recoupling data to suggest that the brickwork alignment is indeed present in the nanosheet structure. However, further ¹³C isotopic labeling of α -carbons at positions 6 and 22 along the B28 backbone and application of PITHIRDS-CT would address the question definitively. If we see a measurable decay then it would indicate there must be an intermolecular contact between the two sites, a positive result for the brickwork arrangement. Isotopic labeling with ¹⁵N and ¹³C at the backbone amide and carbonyl sites of B28 and application of dipolar recoupling NMR could yield estimates for the backbone torsion angles, thereby confirming the proposed folding state of the *cis* Σ -strand. Finally, ¹³C isotopic labeling of a single δ -carbon in a phenylethyl group and application of dipolar recoupling, preferably in the 6-8 site range because it is where we have the most information, may be able to show the presence of a hydrophobic core of the nanosheet. However, because the modeling suggests it is the packing of the

hydrophobic core that enables *cis*-amide bond stability, I believe probing for the hydrophobic core directly to be unnecessary.

It is worth noting that all of these proposed measurements may be inaccessible or limited due to restrictions of available isotopic labeling schemes in peptoids. It is my hope that as the field continues to expand, the need for greater structural knowledge and demonstrated capability of solid-state NMR will push chemists to design synthesis schemes to incorporate ^{13}C and ^{15}N isotopes in any desired pattern.

The most interesting and potentially illuminating of these measurements is, I believe, the measurement of backbone torsion angles. Both the original and updated molecular models show B28 monomers with secondary structure unique from peptide secondary structure. Because of the accessibility of both the *trans* and *cis* configurations of the backbone amide bond, I believe peptoids very likely have a wider array of possible secondary structures than peptides. Classifying these would be a time consuming process because it is unclear at present how many peptoid secondary structures there may be, the forces involved in dictating secondary structure, and the forms of the structures themselves. Fortunately, I believe the peptoid field is here to stay and will continue develop both in its original domain, that of peptide mimics, and as an independent family of designer molecules. As more peptoid systems are developed, we can use NMR to classify secondary structure in peptoids and catalogue the results in the beginnings of a peptoid databank.

At this point, I want to point out that while I do believe peptoid development, and specifically self-assembling peptoid development is a burgeoning field; the cataloguing of peptoid secondary structure and careful design of peptoid primary structure will require

many years to reach a point at which we can accurately predict peptoid structure. We need only look to designer peptide self-assembly to see the difficulty inherent in the task. Designer peptide self-assembly began with the observation that specific patterning of hydrophobicity, hydrophilicity, and electrostatics in the chosen amino acids would yield peptides capable of self-assembly into well-ordered structures. This was an amazing discovery and one that I believe will be remembered as a critical scientific breakthrough in the years and decades to come. However, we must be honest with ourselves in admitting that we as a community have not progressed significantly beyond this point. Others will disagree I am sure, but it is undeniable that we still cannot accurately or reliably predict the atomic-level detail of the assemblies we make. We still design self-assembling peptide systems based on distinct patterning of amino acids, all the while studying naturally occurring self-assembling systems that possess no distinct patterning of amino acids and yet assemble into structures more complex than any we have designed. In the case of peptoids, the lack of reference data from both naturally occurring and designer systems, as well as potentially greater chemical diversity of the peptoid R-groups compared to peptides, mean that the process of developing design protocol and predicting structure in peptoids will only be more difficult. With that said, researchers are already working on the problem and in order to address it we need high-resolution techniques capable of probing peptoid structure. Solid-state NMR is capable of doing just that, and I believe the peptoid field is the much more promising and rich direction for future research for the Paravastu lab in terms of both applications development and toward developing a greater understanding of self-assembly.

5.2 Fmoc-FF

Using solid-state NMR we have shown that Fmoc-FF nanofibers formed in a wide array environmental conditions adopt well-ordered molecular conformations with significant molecular-level polymorphism dependent on the organic solvent used in the self-assembly procedure. From here I was able to use 2D solid-state NMR techniques to identify a backbone hydrogen bonding pattern common to each of the Fmoc-FF assemblies I test in the course of this work.

Moving forward with solid-state NMR in the Fmoc-FF system will be a difficult task. One of the primary reasons for the widespread use of Fmoc-FF as a model LMWG system is its structural simplicity. Unfortunately, structural simplicity leads to fewer distinct chemical shifts in the NMR spectrum. With fewer distinct chemical shifts we would be limited in terms of what information we could extract from the system using 2D correlation NMR experiments. Dipolar recoupling measurements could be used to measure backbone torsion angle of the FF unit of the molecule, though I believe this data would not yield any meaningful insights into the system.

There is one possible avenue which could yield fruitful information for Fmoc-FF and Fmoc-dipeptides as a whole, however. Though we have identified a backbone hydrogen bonding pattern in the FF subunit, we still have no details on what role the Fmoc group plays in maintaining structural integrity of the assembly. We know attachment of the Fmoc group has a substantial effect on assembly properties and behavior, and we know it adopts a well-ordered conformation. I believe we could begin to address knowledge void by synthesizing Fmoc-FF with ^{13}C isotopic labels on the Fmoc group. Commercially, there is very little demand for this level of synthesis. However, if we were able to selectively label with ^{13}C in the Fmoc group, we could then use 2D and dipolar recoupling NMR to

probe for new contacts and estimate distances. This would help answer questions of how the Fmoc groups are oriented in the system and could show whether Fmoc groups interact primarily with one another or if there is any significant interaction with the phenyl rings of the FF subunit. Availability of the isotopic labeling in the Fmoc group, combined with the methods for probing backbone hydrogen bonding I have developed, could lead to a general methodology for determination of structure in Fmoc-dipeptide systems. However, the simplicity of the model system also means there will be a limited number of Fmoc-dipeptide gelators, which may limit broad interest in the topic.

To give you a final, over-arching picture of the thread of my work with Fmoc-FF, I began this believing that it may be an opportunity to find an equilibrium structure in the self-assembled FF subunit of the system. Recall that the Fmoc-FF study timeline began because researchers believed hydrophobic collapse of aromatic residues was crucial to amyloid self-assembly. I thought that if we were able to identify an equilibrium structure in the FF subunit that it might teach us something about the A β structures in Alzheimer's disease. Upon observing molecular-level polymorphism dependent on the assembly environment however, it became clear that we would be able to address no such questions in this study. Additionally, because of my position in the Paravastu Lab I have been privy to many discussions of A β assemblies and analysis of solid-state NMR data of those assemblies. The polymorphic nature of A β assemblies likely leads to many different states in which the FF units of neighboring peptides do not interact, undermining the notion that an equilibrium FF structure would inform on A β . Also, because kinetic trapping is playing such a significant role in peptide assembly, finding an equilibrium FF structure would not be likely to help in identifying kinetically trapped states.

At this point, Fmoc-FF is a prominent LMWG model system, I chose to use it as a means of demonstrating the effectiveness of solid-state NMR. In that regard I succeeded. However, while there is still information we could extract from this system, I do not believe the long-term gains would justify the Paravastu lab's continued pursuit of this project over other available topics.

5.3 Final Summary

Peptoids and LMWG systems appear to be here to stay. Molecules from both systems are being actively investigated for potential use in a wide variety of applications. As our understanding and ambition increase, I believe the applications pursued with these materials will become finer in scope but greater in magnitude. Correctly applying our current understanding of these systems will magnify the effect of ambitious exploration using these systems. That is the niche where my research resides and where we have much work left to do. I do not believe we as a community understand self-assembly nearly as well as what is portrayed in present-day publications. In the mid-nineties we found an amino acid pattern in a single protein that led to self-assembly. To this day, self-assembling peptide designs continue to be based on similar patterning of amino acids, and we are still unable to predict the structures that will form in even these relatively simple systems. To add insult to injury, nature shows us many examples of peptides possessing none of our self-assembly motifs which will assemble into far more intricate structures than what we are able to produce. Now we have expanded into peptoid biology, where we are seeing assemblies and secondary structures that have yet to be observed in peptide systems. We don't even yet know the range of attainable secondary structures available to peptoids. Solid-state NMR possesses all of the tools necessary to address these knowledge gaps. It

will be a painstaking process of iteration, but in time we will be able to achieve it. It is my hope that demonstrating the usefulness of solid-state NMR in this project will help to motivate a continued effort along this path.

The final point I wish to highlight is that this entire project was pushed forward primarily by non-standard applications of solid-state NMR, particularly in the application of PITHIRDS-CT to peptoid B28. Rather than seek out canonical measurements for my target systems (which did not exist for some of my questions), I sought out measurements which would yield information on structure within my systems regardless of their nature. My challenge to future scientists is to continue looking beyond what is standard to find the best means of answering the questions you are faced with. You will have to defend your choices and you will likely be wrong more than you are right, but it is the fastest and surest way to gaining the knowledge you seek.

CHAPTER 6. APPENDIX

6.1 NMR Pulse Sequences

Each pulse sequence is shown with the standard parameter setup used by the Paravastu group.²⁷

6.1.1 CPMAS

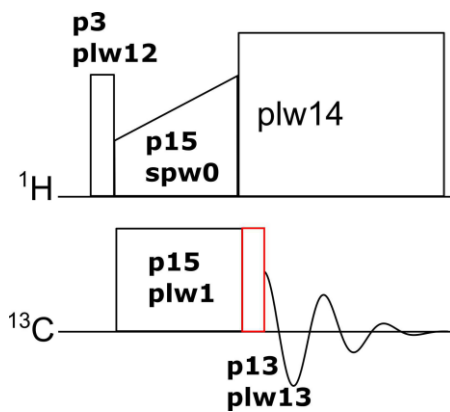


Figure A1 – CPMAS pulse sequence

6.1.2 CHHC

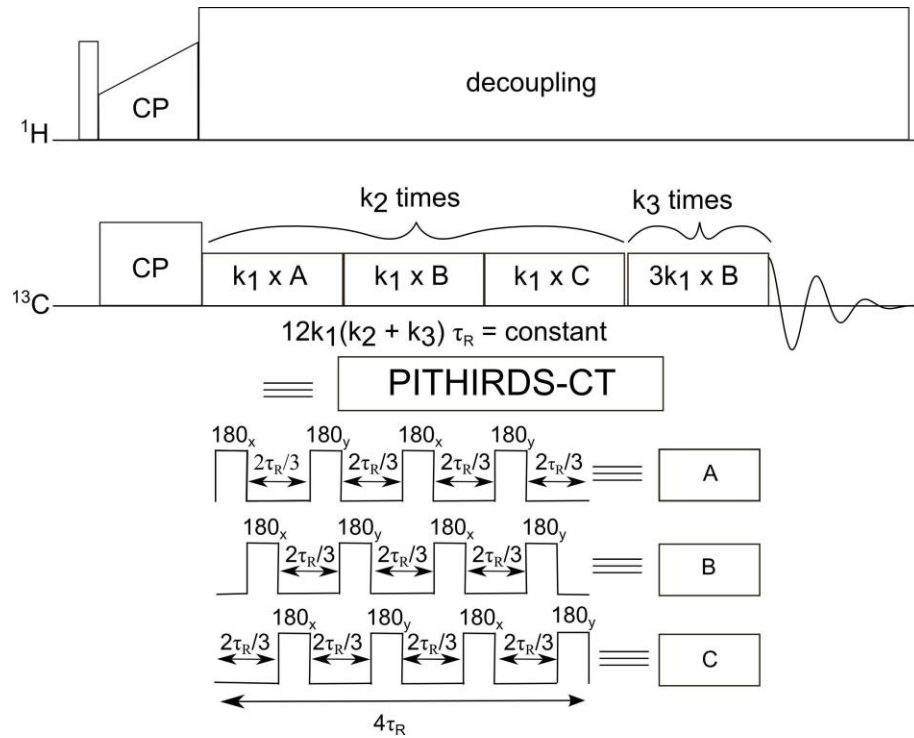


Figure A2 – PITHIRDS-CT pulse sequence

6.1.3 fpRFDR

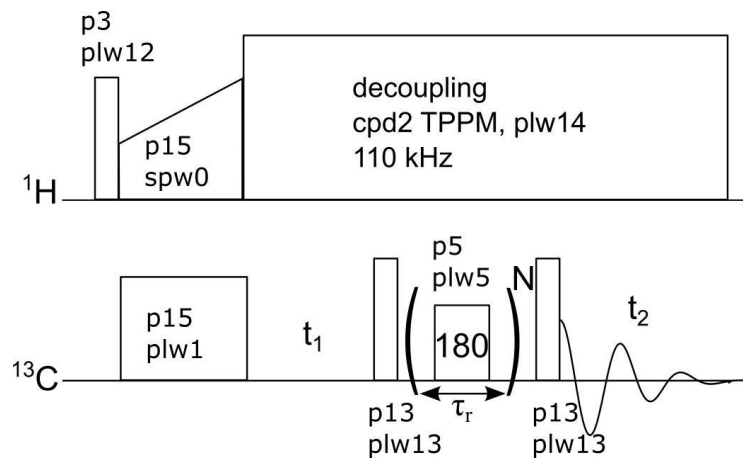


Figure A3 – fpRFDR pulse sequence

6.1.4 CHHC

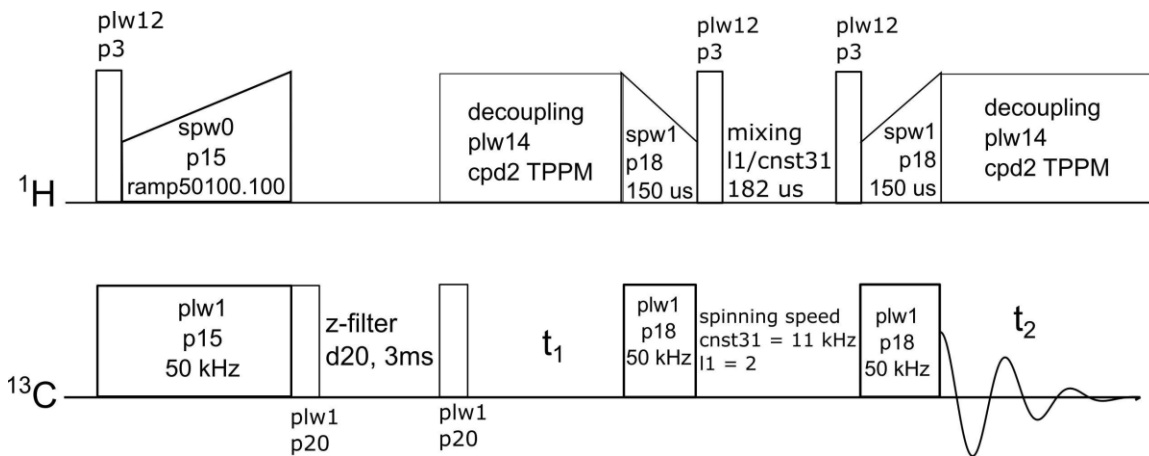


Figure A4 – CHHC pulse sequence

6.2 Peptoid B28 Supplemental Figures

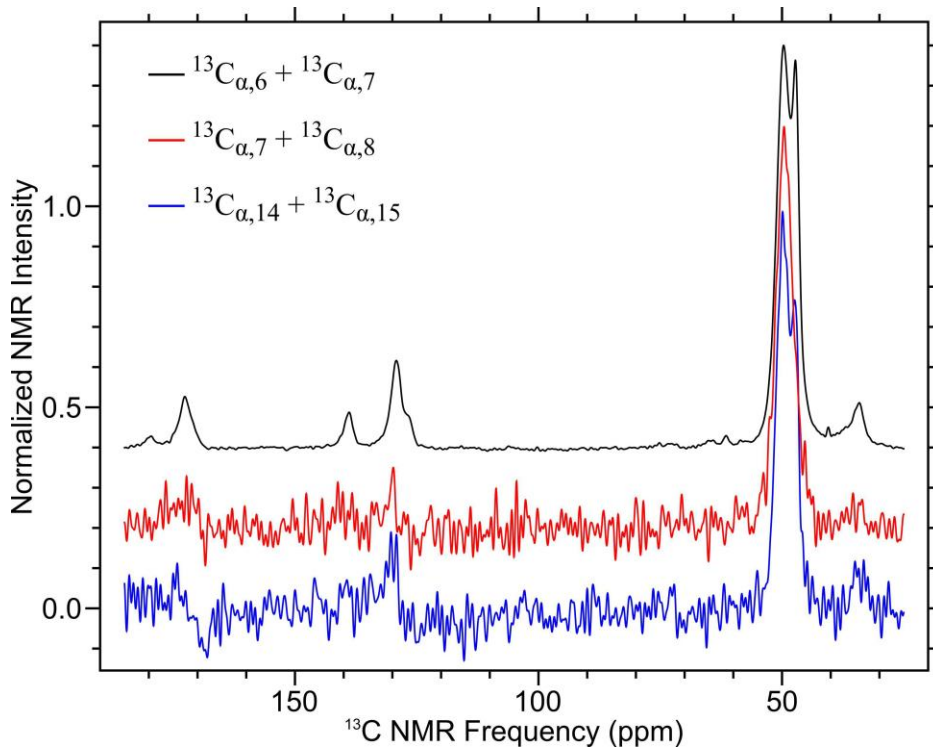


Figure A5 – CPMAS spectra of peptoid B28 nanosheets with 100% ^{13}C isotopic labeling at the sites indicated.

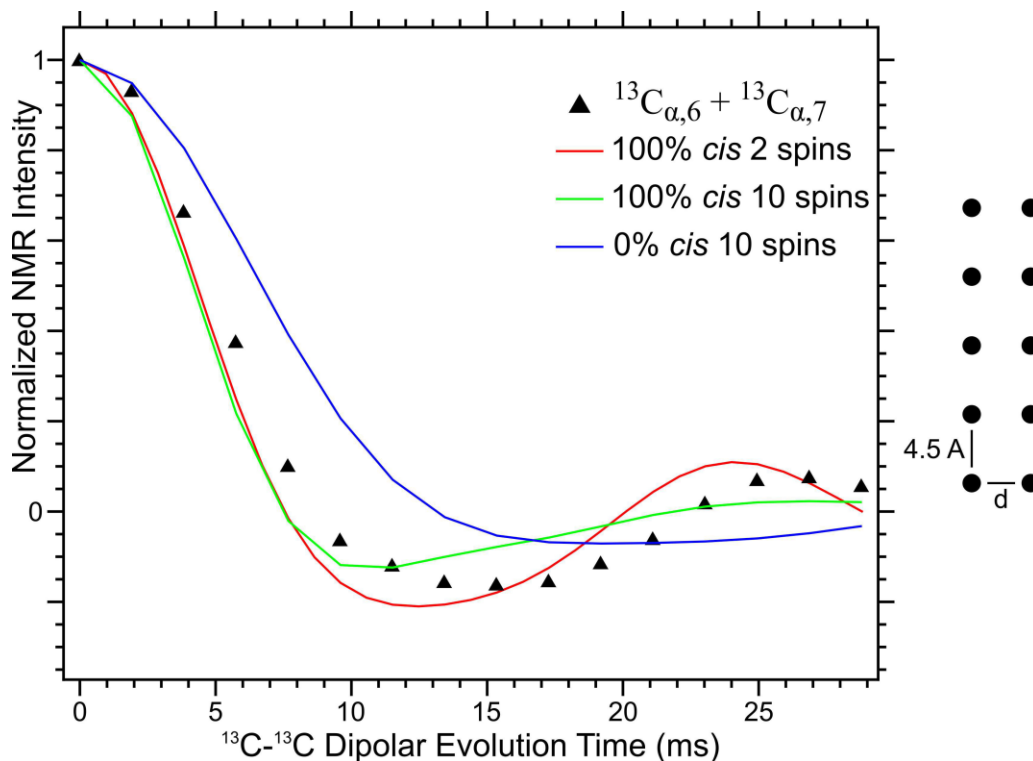


Figure A6 – Comparison of PITHIRDS-CT data to simulated curves that consider potential effects of intermolecular ^{13}C - ^{13}C dipolar couplings. Symbols correspond to measured PITHIRDS-CT decays for peptoid B28 nanosheets labeled at the sixth and seventh α -carbon sites specified in Figure 4. The curve for the 2-spin simulation corresponds to adjacent ^{13}C -atoms on either side of an amide bond in the *cis* configuration, with the distribution of internuclear distances shown in Figure 3. The 10-spin simulations were performed to evaluate the maximum possible effects of inter-molecular ^{13}C - ^{13}C dipolar couplings, and correspond to pairs of ^{13}C atoms separated by an intramolecular distance, d , of either 3\AA (*cis* configuration) or 3.8\AA (*trans* configuration). The 10-spin simulations each include 5 pairs of ^{13}C atoms, with each pair separated by an intermolecular distance of 4.5\AA . The 4.5\AA estimate corresponds to distance between adjacent molecular backbones within the same molecular monolayer observed with aberration-corrected TEM images and x-ray diffraction measurements on similar nanosheet forming peptoids.¹¹ This distance corresponds to a lower limit for intermolecular ^{13}C - ^{13}C distances and therefore maximal possible intermolecular ^{13}C - ^{13}C dipolar couplings. In our view, a 4.5\AA distance between ^{13}C -labeled sites on adjacent molecules corresponds to inter-molecular alignments that are unlikely to occur because like-charged segments of peptoid B28 are unlikely to align in this way. Comparison of the 2-spin and 10-spin simulated PITHIRDS-CT decays indicates that inter-molecular ^{13}C - ^{13}C dipolar couplings did not affect the results for ^{13}C - ^{13}C dipolar recoupling times under 10 ms. Our assessments of amide bond isomerization are thus based on the shapes of curves corresponding to dipolar recoupling times below 10 ms.

6.3 Fmoc-FF Supplemental Figures

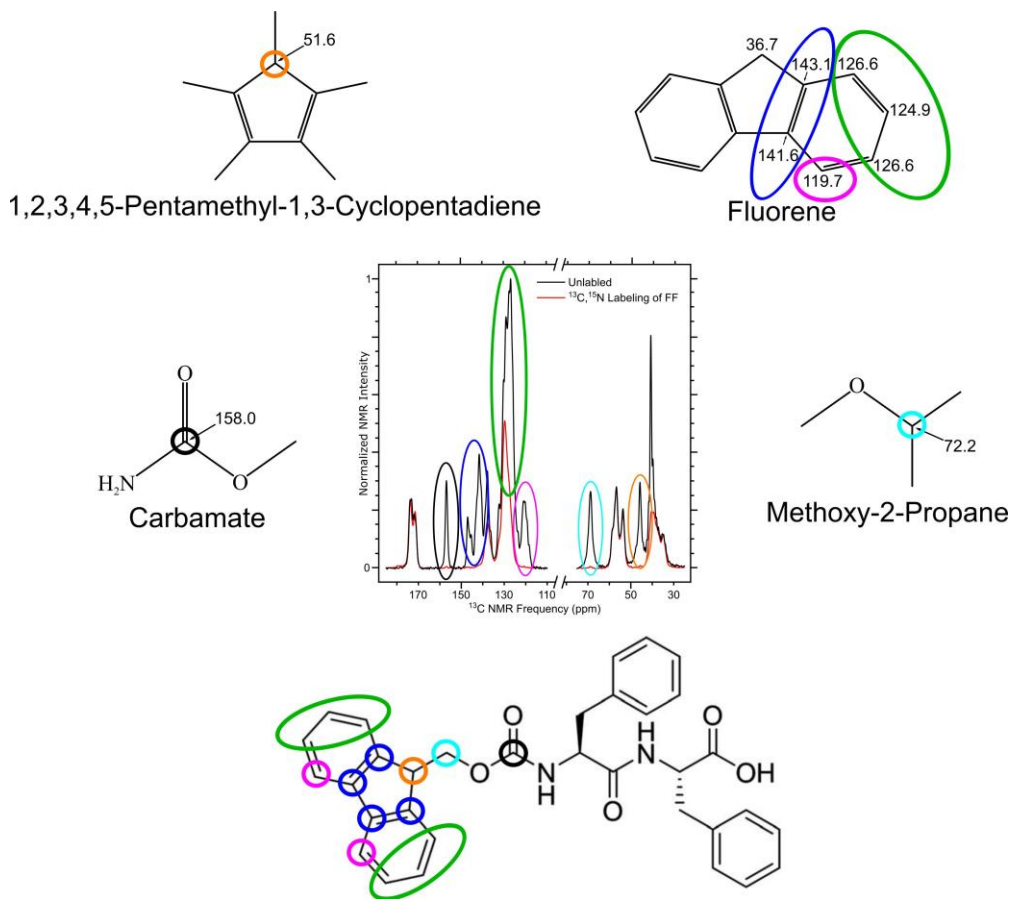


Figure A7 – CPMAS of unlabeled Fmoc-FF (black) and Fmoc-FF with uniform ^{13}C , ^{15}N (red). Both Fmoc-FF samples were assembled in 5% DMSO. Peaks appearing in the black spectrum but not the red spectrum originate from the Fmoc group. They are assigned using chemical shift standards from molecules with similar local chemical bonding.

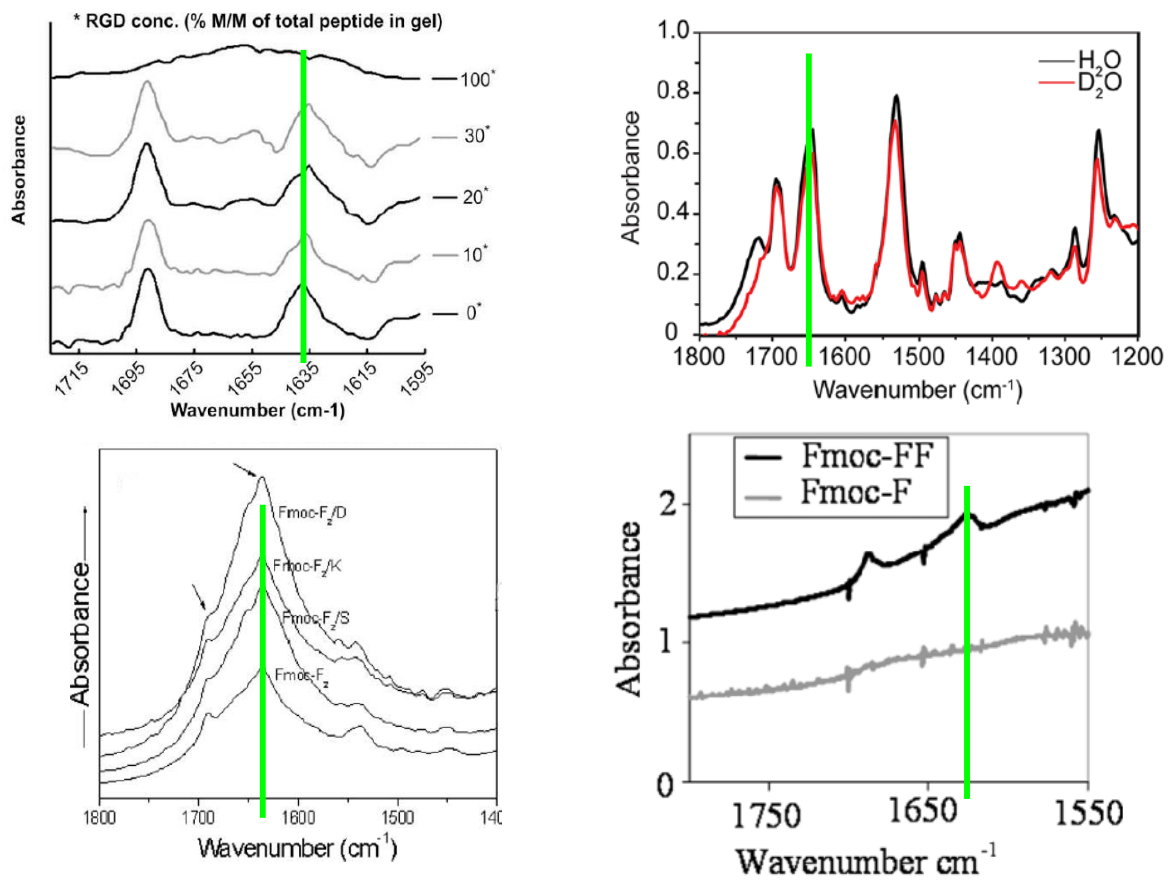


Figure A8 – Reprinted FTIR spectra from Zhou¹⁸ (top left), Ryan²¹ (top right), Jayawarna¹⁶ (bottom left), and Smith³⁵ (bottom right). The green line in each spectrum marks the position of amide I stretch. These spectra were used to conclude that Fmoc-FF forms an anti-parallel β -sheet.

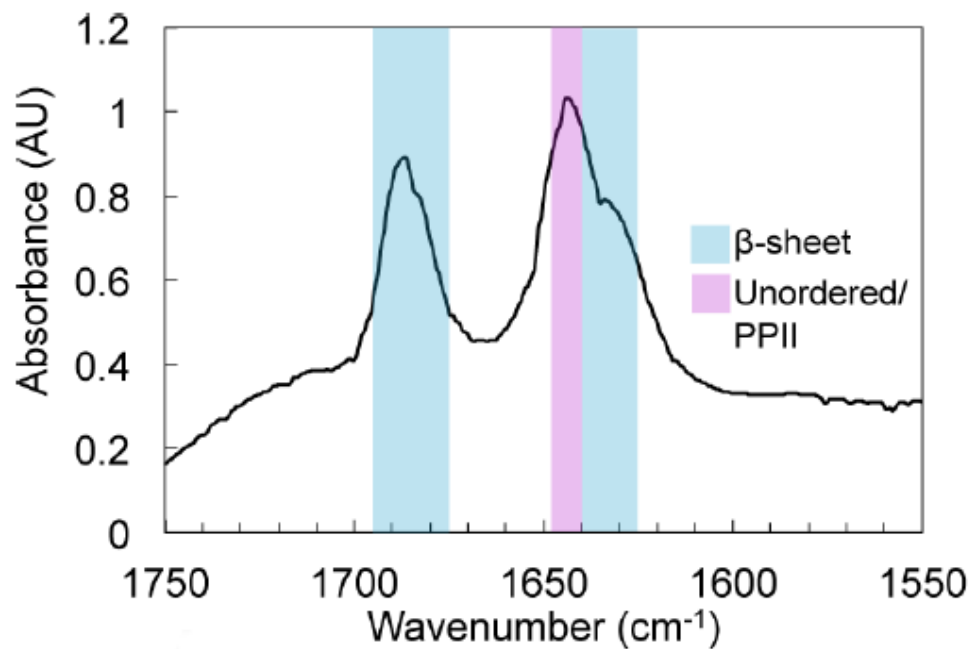


Figure A9 – Reprinted FTIR spectra from Mu⁴⁹. These spectra were used to conclude that Fmoc-FF assemblies are disordered in the FF subunit of the molecule.

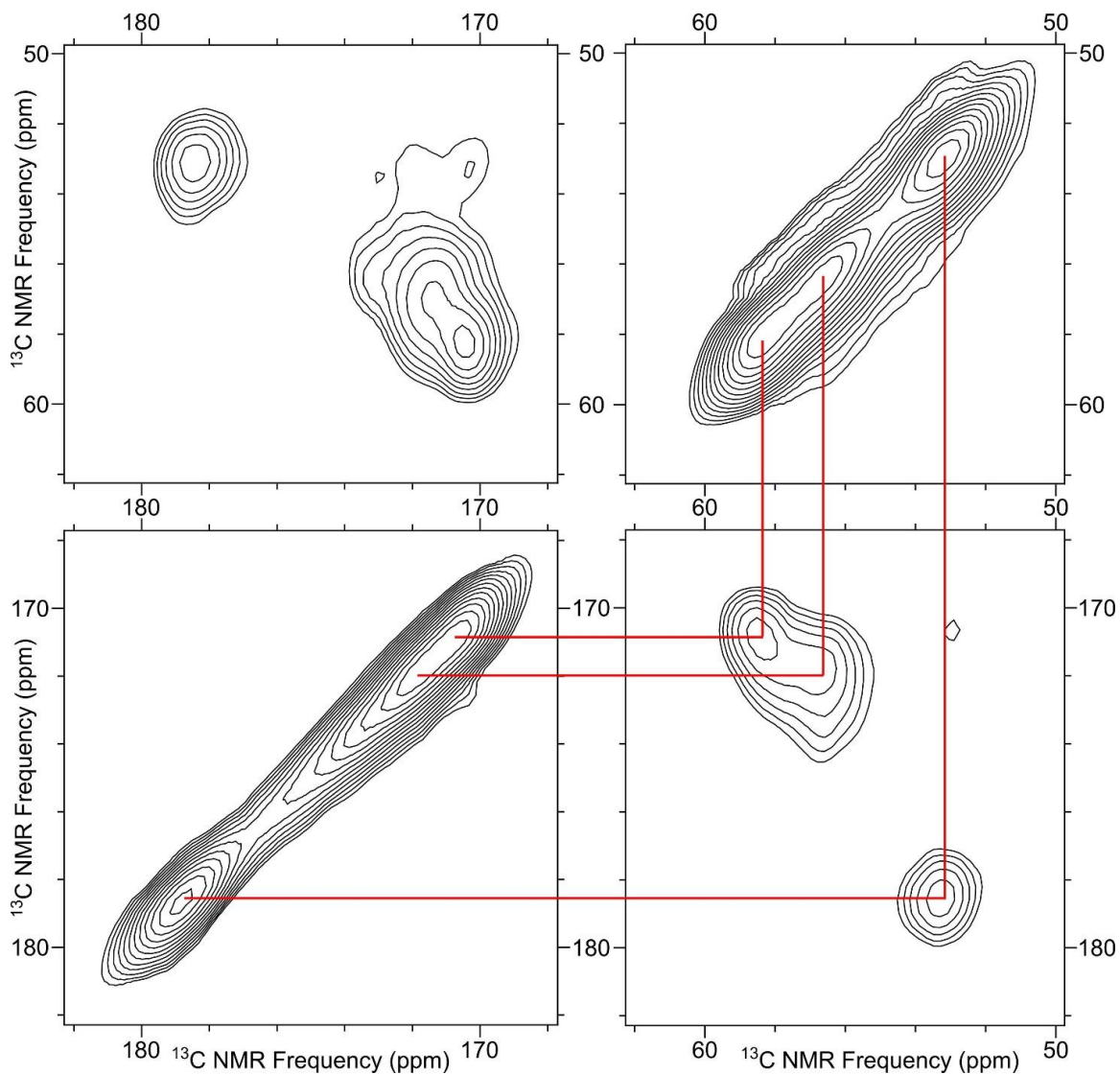


Figure A10 – fpRFDR spectra from Fmoc-FF formed in 10% methanol. The off-diagonal correlation signals indicate that our CHHC contacts are between F1 and F2 of the FF subunit.

REFERENCES

1. Ulrich, E. L.; Akutsu, H.; Doreleijers, J. F.; Harano, Y.; Ioannidis, Y. E.; Lin, J.; Livny, M.; Mading, S.; Maziuk, D.; Miller, Z.; Nakatani, E.; Schulte, C. F.; Tolmie, D. E.; Wenger, R. K.; Yao, H. Y.; Markley, J. L., BioMagResBank. *Nucleic Acids Res.* **2008**, *36*, D402-D408.
2. Garrett, R. H.; Grisham, C. M., *Biochemistry*. Third ed.; Brooks/Cole: Belmont, CA, 2005.
3. Dhouafli, Z.; Cuanalo-Contreras, K.; Hayouni, E. A.; Mays, C. E.; Soto, C.; Moreno-Gonzalez, I., Inhibition of Protein Misfolding and Aggregation by Natural Phenolic Compounds. *Cell. Mol. Life Sci.* **2018**, *75*, 3521-3538.
4. Huang, D.; Zimmerman, M. I.; Martin, P. K.; Nix, A. J.; Rosenberry, T. L.; Paravastu, A. K., Antiparallel beta-Sheet Structure within the C-Terminal Region of 42-Residue Alzheimer's Amyloid-beta Peptides When They Form 150-kDa Oligomers. *J. Mol. Biol.* **2015**, *427* (13), 2319-28.
5. Tay, W. M.; Huang, D.; Rosenberry, T. L.; Paravastu, A. K., The Alzheimer's Amyloid- β (1-42) Peptide Forms Off-Pathway Oligomers and Fibrils that are Distinguished Structurally by Intermolecular Organization. *J. Mol. Biol.* **2013**, *425*, 2494-2508.
6. Zhang, S. G.; Holmes, T.; Lockshin, C.; Rich, A., Spontaneous assembly of a self-complementary oligopeptide to form a stable macroscopic membrane. *P Natl Acad Sci USA* **1993**, *90* (8), 3334-3338.
7. Zhang, S. G.; Lockshin, C.; Herbert, A.; Winter, E.; Rich, A., Zuotin, a putative Z-DNA binding-protein in *Saccharomyces-cerevisiae*. *EMBO J.* **1992**, *11* (10), 3787-3796.
8. Zhang, S. G.; Holmes, T. C.; Dipersio, C. M.; Hynes, R. O.; Su, X.; Rich, A., Self-Complementary Oligopeptide Matrices Support Mammalian-Cell Attachment. *Biomaterials* **1995**, *16* (18), 1385-1393.
9. Simon, R. J.; Kania, R. S.; Zuckermann, R. N.; Huebner, V. D.; Jewell, D. A.; Banville, S.; Ng, S.; Wang, L.; Rosenberg, S.; Marlowe, C. K.; Spellmeyer, D. C.; Tan, R.; Frankel, A. D.; Santi, D. V.; Cohen, F. E.; Bartlett, P. A., Peptoids - A Modular Approach To Drug Discovery. *PNAS* **1992**, *89* (20), 9367-9371.
10. Reches, M.; Gazit, E., Self-Assembly of Peptide Nanotubes and Amyloid-Like Structures By Charged-Termini-Capped Diphenylalanine Peptide Analogues. *Isr. J. Chem.* **2005**, *45* (3), 363-371.
11. Nam, K. T.; Shelby, S. A.; Choi, P. H.; Marciel, A. B.; Chen, R.; Tan, L.; Chu, T. K.; Mesch, R. A.; Lee, B.; Connolly, M. D.; Kisielowski, C.; Zuckermann, R. N., Free-

Floating Ultrathin Two-Dimensional Crystals from Sequence-Specific Peptoid Polymers. *Nature Materials* **2010**, *9* (5), 454-460.

12. Seurnyck, S. L.; Patch, J. A.; Barron, A. E., Simple, Helical Peptoid Analogs of Lung Surfactant Protein B. *Chem. Biol.* **2005**, *12* (1), 77-88.

13. Wu, C. W.; Seurnyck, S. L.; Lee, K. Y. C.; Barron, A. E., Helical Peptoid Mimics of Lung Surfactant Protein C. *Chem. Biol.* **2003**, *10* (11), 1057-1063.

14. Robertson, E. J.; Battigelli, A.; Proulx, C.; Mannige, R. V.; Haxton, T. K.; Yun, L.; Whitlam, S.; Zuckermann, R. N., Design, Synthesis, Assembly, and Engineering of Peptoid Nanosheets. *Acc. Chem. Res.* **2016**, *49* (3), 379-389.

15. Draper, E. R.; Adams, D. J., Low-Molecular-Weight Gels: The State of the Art. *Chem* **2017**, *3*, 390-410.

16. Jayawarna, V.; Richardson, S. M.; Hirst, A. R.; Hodson, N. W.; Saiani, A.; Gough, J. E.; Ulijn, R. V., Introducing Chemical Functionality in Fmoc-Peptide Gels for Cell Culture. *Acta Biomater.* **2009**, *5*, 934-943.

17. Jayawarna, V.; Ali, M.; Jowitt, T. A.; Miller, A. E.; Saiani, A.; Gough, J. E.; Ulijn, R. V., Nanostructured hydrogels for three-dimensional cell culture through self-assembly of fluorenylmethoxycarbonyl-dipeptides. *Adv. Mater.* **2006**, *18* (5), 611-+.

18. Zhou, M.; Smith, A. M.; Das, A. K.; Hodson, N. W.; Collins, R. F.; Ulijn, R. V.; Gough, J. E., Self-Assembled Peptide-Based Hydrogels As Scaffolds for Anchorage-Dependent Cells. *Biomaterials* **2009**, *30*, 2523-2530.

19. Alakpa, E. V.; Jayawarna, V.; Lampel, A.; Burgess, K. V.; West, C. C.; Bakker, S. C. J.; Roy, S.; Javid, N.; Fleming, S.; Lamprou, D. A.; Yang, J.; Miller, A.; Urquhart, A. J.; Frederix, P. W. J. M.; Hunt, N. T.; Peault, B.; Ulijn, R. V.; Dalby, M. J., Tunable Supramolecular Hydrogels for Selection of Lineage-Guiding Metabolites in Stem Cell Cultures. *Chem* **2016**, *1*, 298-319.

20. Wang, Y.; Lin, S.; Nelli, S. R.; Zhan, F.; Cheng, H.; Lai, T.; Yeh, M.; Lin, H.; Hung, S., Self-Assembled Peptide-Based Hydrogels as Scaffolds for Proliferation and Multi-Differentiation of Mesenchymal Stem Cells. *Macromol. Biosci.* **2017**, *17*, 1600192 (1-13).

21. Ryan, K.; Beirne, J.; Redmond, G.; Kilpatrick, J. I.; Guyonnet, J.; Buchete, N.; Kholkin, A. L.; Rodriguez, B. J., Nanoscale Piezoelectric Properties of Self-Assembled Fmoc-FF Peptide Fibrous Networks. *Applied Materials and Interfaces* **2015**, *7*, 12702-12707.

22. Xu, H.; Das, A. K.; Horie, M.; Shaik, M. S.; Smith, A. M.; Luo, Y.; Lu, X.; Collins, R. F.; Liem, S. Y.; Song, A.; Popelier, P. L. A.; Turner, M. L.; Xiao, P.; Kinloch, I. A.; Ulijn, R. V., An Investigation of the Conductivity of Peptide Nanotube Networks Prepared by Enzyme-Triggered Self-Assembly. *Nanoscale* **2010**, *2*, 960-966.

23. Ischakov, R.; Adler-Abramovich, L.; Buzhansky, L.; Shekhter, T.; Gazit, E., Peptide-Based Hydrogel Nanoparticles as Effective Drug Delivery. *Biorg. Med. Chem.* **2013**, *21*, 3517-3522.
24. Skilling, K. J.; Citossi, F.; Bradshaw, T. D.; Ashford, M.; Kellam, B.; Marlow, M., Insights into Low Molecular Mass Organic Gelators: a Focus on Drug Delivery and Tissue Engineering Applications. *Soft Matter* **2014**, *10*, 237-256.
25. Eskandari, S.; Guerin, T.; Toth, I.; Stephenson, R. J., Recent Advances in Self-Assembled Peptides: Implications for Targeted Drug Delivery and Vaccine Engineering. *Adv. Drug Del. Rev.* **2017**, *110*, 169-187.
26. Harper, M. M.; Connolly, M. L.; Goldie, L.; Irvine, E. J.; Shaw, J. E.; Jayawarna, V.; Richardson, S. M.; Dalby, M. J.; Ulijn, R. V., Biogelx: Cell Culture on Self-Assembling Peptide Gels. In *Peptide Self-Assembly*, Nilsson, B.; Doran, T., Eds. Humana Press: New York, NY, 2018; pp 23-68.
27. D., H.; Hudson, B. C.; Gao, Y.; Roberts, E. K.; Paravastu, A. K., Solid-State NMR Structural Characterization of Self-Assembled Peptides with Selective ¹³C and ¹⁵N Isotopic Labels. In *Peptide Self-Assembly*, Nilsson, B.; Doran, T., Eds. Humana Press: New York, NY, 2018; pp 23-68.
28. Pines, A.; Waugh, J. S.; Gibby, M. G., PROTON-ENHANCED NUCLEAR INDUCTION SPECTROSCOPY - METHOD FOR HIGH-RESOLUTION NMR OF DILUTE SPINS IN SOLIDS. *J. Chem. Phys.* **1972**, *56* (4), 1776-&.
29. Tycko, R., Symmetry-based constant-time homonuclear dipolar recoupling in solid state NMR. *J. Chem. Phys.* **2007**, *126* (6), 064506 (1-9).
30. Tycko, R.; Ishii, Y., Constraints on supramolecular structure in amyloid fibrils from two-dimensional solid-state NMR spectroscopy with uniform isotopic labeling. *J. Am. Chem. Soc.* **2003**, *125* (22), 6606-6607.
31. Veshtort, M.; Griffin, R. G., SPINEVOLUTION: A powerful tool for the simulation of solid and liquid state NMR experiments. *J. Magn. Reson.* **2006**, *178* (2), 248-282.
32. Robertson, E. J.; Proulx, C.; Su, J. K.; Garcia, R. L.; Yoo, S.; Nehls, E. M.; Connolly, M. D.; Taravati, L.; Zuckermann, R. N., Molecular Engineering of the Peptoid Nanosheet Hydrophobic Core. *Langmuir* **2016**, *32*, 11946-11957.
33. Phillips, J. C.; Braun, R.; Wang, W.; Gumbart, J.; Tajkhorshid, E.; Villa, E.; Chipot, C.; Skeel, R. D.; Kale, L.; Schulten, K., Scalable molecular dynamics with NAMD. *J. Comput. Chem.* **2005**, *26* (16), 1781-1802.
34. Mirijanian, D. T.; Mannige, R. V.; Zuckermann, R. N.; Whitelam, S., Development and Use of an Atomistic CHARMM-Based Forcefield for Peptoid Simulation. *J. Comput. Chem.* **2014**, *35*, 360-370.

35. Smith, A. M.; Williams, R. J.; Tang, C.; Coppo, P.; Collins, R. F.; Turner, M. L.; Saiani, A.; Ulijn, R. V., Fmoc-Diphenylalanine Self Assembles to a Hydrogel via a Novel Architecture Based on π - π Interlocked β -Sheets. *Adv. Mater.* **2008**, *20* (1), 37-41.
36. Mannige, R. V.; Whitelam, S.; al., E., Peptoid nanosheets exhibit a new secondary-structure motif. *Nature* **2015**, *526*, 415-420.
37. Kabiri, M.; Bushnak, I.; McDermot, M. T.; Unsworth, L. D., Toward a Mechanistic Understanding of Ionic Self-Complementary Peptide Self-Assembly: Role of Water Molecules and Ions. *Biomacromolecules* **2013**, *14*, 3943-3950.
38. Edison, J. R.; Spencer, R. K.; Butterfoss, G. L.; Hudson, B. C.; Hochbaum, A. I.; Paravastu, A. K.; Zuckermann, R. N.; Whitelam, S., Conformations of Peptoids in Nanosheets Result from the Interplay of Backbone Energetics and Intermolecular Interactions. *Proceedings of the National Academy of Sciences* **2018**, *115*, 5647-5651.
39. Sui, Q.; Borchardt, D.; Rabenstein, D. L., Kinetics and Equilibria of Cis/Trans Isomerization of Backbone Amide Bonds in Peptoids. *J. Am. Chem. Soc.* **2007**, *129* (39), 12042-12048.
40. Dudukovic, N. A.; Zukoski, C. F., Gelation of Fmoc-diphenylalanine is a First Order Phase Transition. *Soft Matter* **2015**, *11* (38), 7663-7673.
41. Raeburn, J.; Mendoza-Cuenca, C.; Cattoz, B. N.; Little, M. A.; Terry, A. E.; Cardoso, A. Z.; Griffiths, P. C.; Adams, D. J., The Effect of Solvent Choice on the Gelation and Final Hydrogel Properties of Fmoc-diphenylalanine. *Soft Matter* **2015**, *11*, 927-935.
42. Bowerman, C. J.; Nilsson, B. L., Self-Assembly of Amphipathic β -Sheet Peptides: Insights and Applications. *Peptide Science* **2012**, *98* (3), 169-184.
43. Gazit, E., A Possible Role for Pi-Stacking in the Self-Assembly of Amyloid Fibrils. *FASEB* **2002**, *16*, 77-83.
44. Reches, M.; Gazit, E., Casting metal nanowires within discrete self-assembled peptide nanotubes. *Science* **2003**, *300* (5619), 625-627.
45. Gorbitz, C. H., Nanotube Formation by Hydrophobic Dipeptides. *Chemistry -- A European Journal* *7*, 5153-5159.
46. Dudukovic, N. A.; Zukoski, C. F., Mechanical Properties of Self-Assembled Fmoc-Diphenylalanine Molecular Gels. *Langmuir* **2014**, *30* (15), 4493-4500.
47. Greenfield, N. J., Applications of circular dichroism in protein and peptide analysis. *TrAC, Trends Anal. Chem.* **1999**, *18* (4), 236-244.
48. Sitsanidis, E. D.; Piras, C. C.; Alexander, B. D.; Siligardi, G.; Javorfi, T.; Hall, A. J.; Edwards, A. A., Circular Dichroism Studies of Low Molecular Weight Gelator

Hydrogelators: The Use of SRCD and Addressing Practical Issues. *Chirality* **2018**, *30* (6), 708-718.

49. Mu, X.; Eckes, K. M.; Nguyen, M. M.; Suggs, L. J.; Ren, P., Experimental and Computational Studies Reveal and Alternative Supramolecular Structure for Fmoc-Dipeptide Self-Assembly. *Biomacromolecules* **2012**, *13*, 3562-3571.

50. Tatulian, S. A., Structural Characterization of Membrane Proteins and Peptides by FTIR and ATR-FTIR Spectroscopy. In *Lipid-Protein Interactions, Methods and Protocols*, Kleinschmidt, J. H., Ed. Springer Science+Business Media: New York, 2013; Vol. 974.

51. Fleming, S.; Frederix, P. W. J. M.; Sasselli, I. R.; Hunt, N. T.; Ulijn, R. V.; Tuttle, T., Assessing the Utility of Infrared Spectroscopy as a Structural Diagnostic Tool for β -Sheets in Self-Assembling Aromatic Peptide Amphiphiles. *Langmuir* **2013**, *29*, 9510-9515.

52. Kodali, R.; Williams, A. D.; Chemuru, S.; Wetzel, R., Abeta(1-40) forms five distinct amyloid structures whose beta-sheet contents and fibril stabilities are correlated. *J. Mol. Biol.* **2010**, *401* (3), 503-17.

53. Kodali, R.; Wetzel, R., Polymorphism in the intermediates and products of amyloid assembly. *Curr. Opin. Struct. Biol.* **2007**, *17* (1), 48-57.

54. Tang, C.; Smith, A. M.; Collins, R. F.; Ulijn, R. V.; Saiani, A., Fmoc-Diphenylalanine Self-Assembly Mechanism Induces Apparent pKa Shifts. *Langmuir* **2009**, *25* (16), 9447-9453.

55. Wang, J.; Liu, K.; Yan, L.; Wang, A.; Bai, S.; Yan, X., Trace Solvent as a Predominant Factor to Tune Dipeptide Self-Assembly. *ACS Nano* **2016**, *10*, 2138-2143.

56. Reich, H. J. C-13 Chemical Shifts. <http://www.chem.wisc.edu/areas/reich/nmr/c13-data/cdata.htm>.

57. Rajbhandary, A.; Nilsson, B. L., Investigating the Effects of Peptoid Substitutions in Self-Assembly of Fmoc-Diphenylalanine. *Peptide Science* **2017**, *108* (2), 1-11.